Supporting Information

Protease-responsive peptide-conjugated mitochondrial-targeting AIEgens for selective imaging and inhibition of SARS-CoV-2-infected cells

Yong Cheng,[1] Alex E. Clark,[2] Jiajing Zhou,[1] Tengyu He,[3] Yi Li,[1] Raina M. Borum,[1] Matthew N. Creyer,[1] Ming Xu,[1] Zhicheng Jin,[1] Jingcheng Zhou,[1] Wonjun Yim,[3] Zhuohong Wu,[1] Pavla Fajtová,[4] Anthony J. O'Donoghue,[4] Aaron F. Carlin,[2] Jesse V. Jokerst[1, 3, 5]*

[1]Department of NanoEngineering, University of California, San Diego, La Jolla, CA 92093, USA

[2]Department of Medicine, University of California, San Diego, La Jolla, CA 92037, USA

[3]Materials Science and Engineering Program, University of California, San Diego, La Jolla, CA 92093, USA

[4]Skaggs School of Pharmacy and Pharmaceutical Sciences, University of California, San Diego, La Jolla, CA 92093, USA

[5]Department of Radiology, University of California, San Diego, La Jolla, CA 92093, USA

✉E-mail: jjokerst@eng.ucsd.edu

Table of Contents

References

Supplementary Movies

Supplementary Movie S1

Description: SARS-CoV-2 infected TMPRSS2-Vero cells incubated with PSGMR, Hoechst 33258, PI, and Alexa 488 for nucleocapsid (Turn around X-axis).

Supplementary Movie S2

Description: SARS-CoV-2 infected TMPRSS2-Vero cells incubated with PSGMR, Hoechst 33258, PI, and Alexa 488 for nucleocapsid (Z-axis scanning).

Supplementary Movie S3

Description: SARS-CoV-2 infected TMPRSS2-Vero cells incubated with PSGMR, Hoechst 33258, PI, and Alexa 488 for M^{pro} (Turn around X-axis).

Supplementary Movie S4

Description: SARS-CoV-2 infected TMPRSS2-Vero cells incubated with PSGMR, Hoechst 33258, PI, and Alexa 488 for M^{pro} (Z-axis scanning).

1. Materials and methods.

Rink-amide resin (particle size 100 to 150 mesh; loading 0.67 mmol/g), Fmoc-protected L-amino acids, and O-benzotriazole-N, N, N', N'-tetramethyl-uronium-hexafluorophosphate (HBTU) were purchased from AAPPTec, LLC. (Kentucky, USA). The 4-(1,2,2-triphenylvinyl) benzaldehyde, 1,4-dibromobutane, 4-methylpyrdine, Hoechst 33258, and propidium iodide (PI) were purchased from Combi-Blocks, Inc. (San Diego, USA). Tris-(hydroxymethyl) aminomethane (Tris-base), tris-(hydroxymethyl) aminomethane hydrochlorideand (Tris-HCl), sodium azide, sodium ascorbate, copper (I) iodide, N, N-diisopropylethylamine (DIPEA), thrombin, hemoglobin, albumin bovine serum, lipopolysaccharide, and resazurin based in vitro toxicology assay kit were purchased from Sigma-Aldrich (Missouri, USA). CGAVLQDDD, AVLQFFVLKC, RVRRSAVLQSGFRKMAC, and CGKLVFFGTSAVLQSGFRGDDD were purchased from Genscript Inc. (New Jersey, USA).

The SARS-CoV-2 M^{pro} expression plasmid was provided to us from Dr. Rolf Hilgenfeld, University of Lübeck, Germany. Recombinant SARS-CoV-2 M^{pro} was expressed and purified as described previously in 20 mM Tris-HCl buffer (pH 8.0) with 150 mM NaCl, 1 mM DTT, and 5 % glycerol.[1] A SARS-CoV-2 M^{pro} plasmid, an influenza virus protein (A/PR8/1834 NP, PR8 in short) plasmid, and a M^{pro}-related FlipGFP reporter plasmid were a kind gift from Nicholas S. Heaton.[2] M^{pro} inhibitor GC376 was purchased from Selleckchem, LLC. (Houston, USA). HEK 293T cells were a kind gift from Dr. Liangfang Zhang. All other reagents were obtained from commercial sources and used without further purification. Deionized water (18.2 MΩ·cm) used in all experiments was purified with a Milli-Q Academic water purification system (Millipore Corp., Billerica, MA, USA).

Peptides were synthesized using an AAPPTec Eclipse system through standard solid phase Fmoc syntheses on rink-amide resin. Electrospray ionization mass spectrometry (ESI-MS) data was acquired by using a Micromass Quattro Ultima mass spectrometer. High resolution mass spectra (HRMS) were recorded on a Bruker microTOF II mass spectrometer system. High performance liquid chromatography (HPLC) was performed by using a Shimadzu LC-40 HPLC system under the wavelength of 195 nm, 254 nm, and 405 nm. The sample was dissolved in water or acetonitrile, applied on a Zorbax 300 BS C18 column (5 um, 9.4x250mm) from Agilent, and eluted at 1.5 mL/min with a 40 min gradient from 10% to 95% solvent B where solvent A is water (0.05% TFA solution) and solvent B is acetonitrile (0.05% TFA solution). All products were purified by HPLC to reach a purity of 90%. UV-Vis absorption and fluorescence spectra were performed on a Synergy H1 microplate reader (BioTek). Confocal laser scanning microscopy images were obtained on a Zeiss LSM880 confocal laser scanning microscope (Zeiss) at the school of medicine microscopy and histology core of University of California San Diego. Dynamic light scattering (DLS) measurements were performed on a Malvern NANO-ZS90 Zetasizer to determine hydrodynamic sizes and zeta potential values of the nanosystems studied. Transmission electron microscopy (TEM) images were acquired using an FEI Tecnai F20 instrument at an operation voltage of 200 kV. Circular dichroism (CD) experiments were performed on a CD spectrometer (AVIV, Model 215) using 2 mm quartz slides at 25 °C. Flow cytometric analysis was carried out under a flow cytometer (BD LSR Fortessa).

2. Molecular design and imaging mechanism.

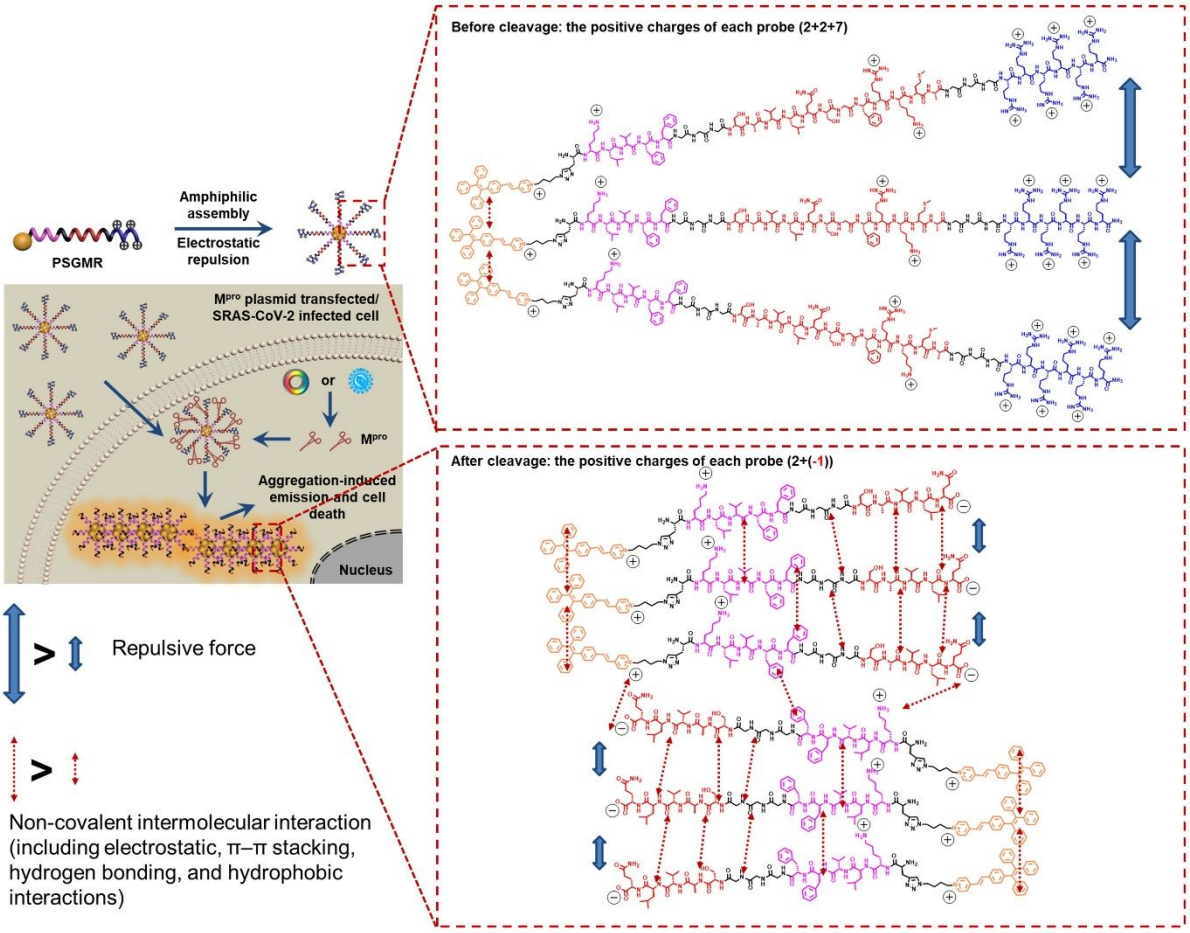

Scheme S1. The mechanism of PSGMR was used for selective imaging and inhibition of M^{pro} plasmid-transfected or SARS-CoV-2-infected cells. The amphipathic PSGMR has 13 positive charges and can form loose nanoparticles due to the electrostatic repulsion. After cleavage by M^{pro} and the absence of cationic polypeptides, the resulting PSG has four positive charges and a C-terminal carboxyl group to decrease the electrostatic repulsion and enhance the molecular interactions. The electrostatic attraction, decreased hydrophilicity, and increased self-assembly all increase aggregation of PSG to form nanofibers with strong yellow fluorescence.

SARS-CoV-2 M^{pro} sequence:[3]

SGFRKMAFPSGKVEGCMVQVTCGTTTLNGLWLDDVVYCPRHVICTSEDMLNPNYED
LLIRKSNHNFLVQAGNVQLRVIGHSMQNCVLKLKVDTANPKTPKYKFVRIQPGQTFS
VLACYNGSPSGVYQCAMRPNFTIKGSFLNGSCGSVGFNIDYDCVSFCYMHHMELPTG
VHAGTDLEGNFYGPFVDRQTAQAAGTDTTITVNVLAWLYAAVINGDRWFLNRFTTT
LNDFNLVAMKYNYEPLTQDHVDILGPLSAQTGIAVLDMCASLKELLQNGMNGRTIL
GSALLEDEFTPFDVVRQCSGVTFQ

3. Synthesis and Characterization

(1) PyTPE synthesis:[4, 5] PyTPE was synthesized according to our previous reports and the procedures in the literatures.

(2) Crude peptide synthesis: 100 mg rink amide resin was chosen in solid-phase peptide synthesis. 2 x 4 mL 20% piperidine in DMF, 0.1 M amino acid in 3 mL DMF (5 equivalents), 0.1 M HBTU in 3 mL DMF (5 equivalents), and 0.2 M DIPEA in 3 mL DMF (10 equivalents) were used for each coupling cycle under the protection of nitrogen. After the completion of solid phase synthesis, peptides were cleaved of the resins by treating with cleavage cocktail containing 2.5 % thioanisole, 3% TIPS, 2.5% water, and 92% TFA for 3 hours followed by filtration to remove resin. Peptides were precipitated and centrifuged by addition of ice-cold diethyl ether to the filtrates. The residue was dissolved in 5 mL MeCN/H_2O (v/v=1:1) solution and lyophilized. Crude peptides were purified using semi-preparative HPLC.

(3) Coupling with PyTPE:[4, 5] PyTPE (5.0 mg, 7.1 μmol), sodium ascorbate (0.7 mg, 3.6 μmol), copper (I) iodide (0.7 mg, 3.6 μmol), and the purified peptide (3.6 μmol) were dissolved in DMSO/H2O (v/v=1:1) solution, and stirred at 50 ^{0}C for 24 h under protection of nitrogen. The crude probes were purified using semi-preparative HPLC.

3.1 Synthesis of PyTPE.

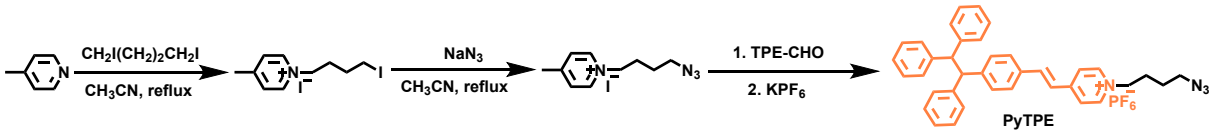

Scheme S2. The synthetic route of PyTPE.

The main synthetic route of PyTPE is three steps: (a) Synthesis of Py-I. (b) Synthesis of Py-N_3, (c) Synthesis of PyTPE, HRMS (ESI) of PyTPE m/z: $[M]^+$ calcd. for 533.2700; found, 533.3771.

3.2 Synthesis of PSMR.

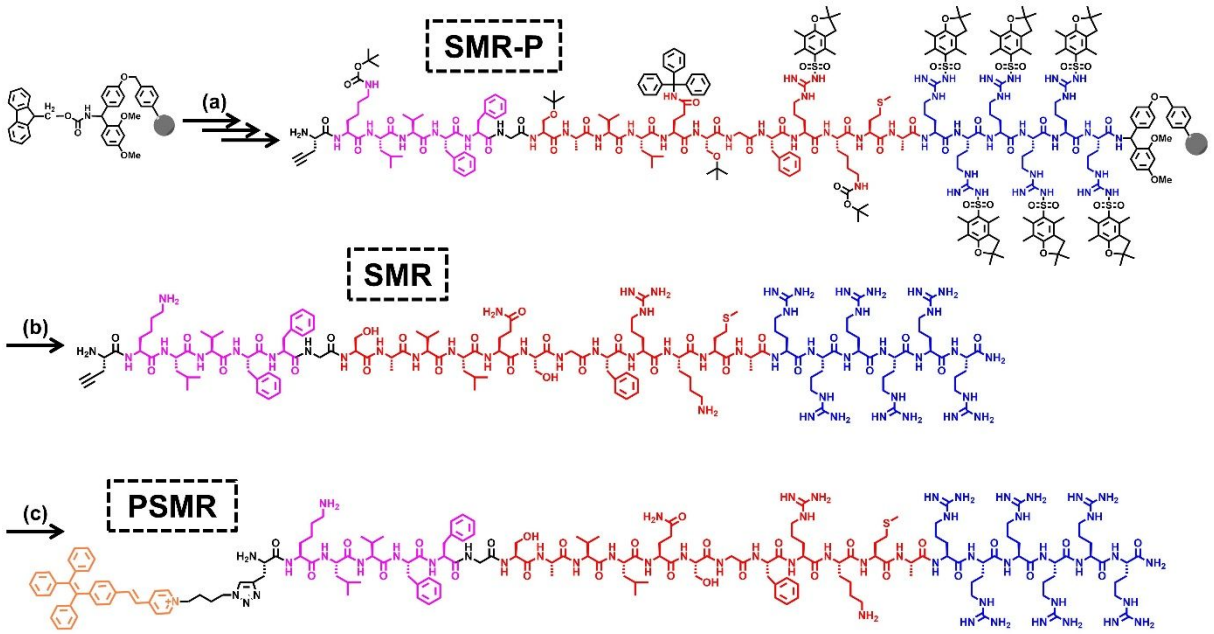

Scheme S3. The synthetic route of PSMR.

The main synthetic route of PSMR is three steps through standard solid phase Fmoc synthesis and copper-catalyzed azide-alkyne click reaction: (a) Synthesis of SMM-P. (b) Synthesis of SMR, HRMS (ESI) m/z: $[M+4H]^{4+}/4$ calcd. for 754.9458; found, 755.5761. $[M+5H]^{5+}/5$ calcd. for 604.1582; found, 604.6490. $[M+6H]^{6+}/6$ calcd. for 503.6331; found, 504.0028. (c) Synthesis of PSMR, HRMS (ESI) m/z: $[M+4H]^{4+}/4$ calcd. for 888.2633; found, 888.6069. $[M+5H]^{5+}/5$ calcd. for 710.8122; found, 711.2593. $[M+6H]^{6+}/6$ calcd. for 592.5115; found, 592.8325. $[M+7H]^{7+}/7$ calcd. for 508.0109; found, 508.3657.

3.3 Synthesis of PSGMR.

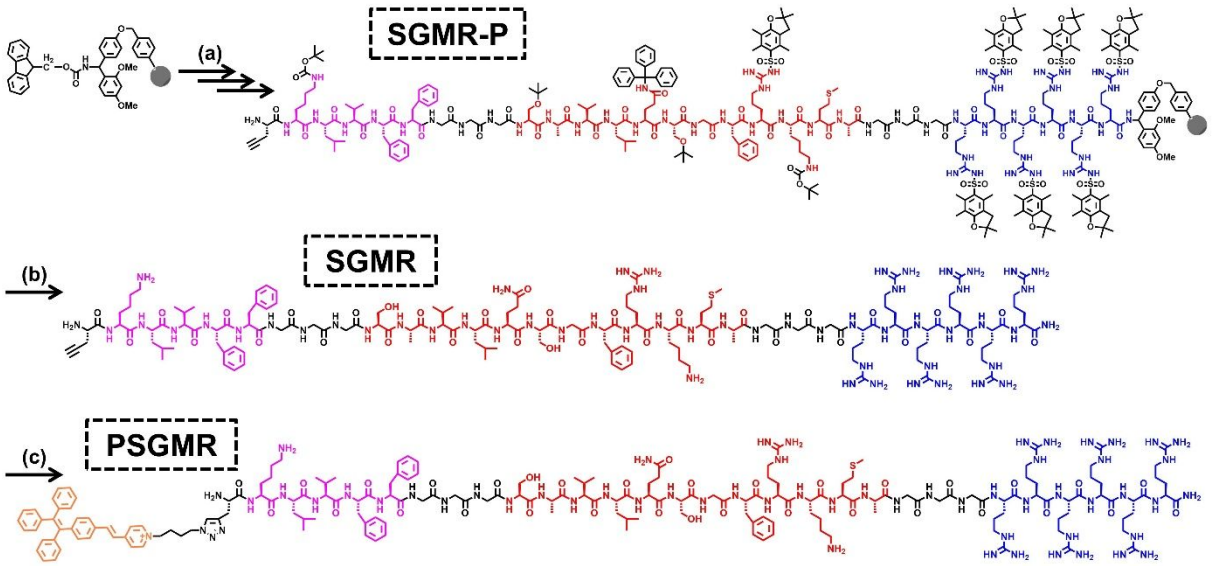

Scheme S4. The synthetic route of PSGMR.

The main synthetic route of PSGMR is three steps through standard solid phase Fmoc synthesis and copper-catalyzed azide-alkyne click reaction. (a) Synthesis of SGMR-P. (b) Synthesis of SGMR, HRMS (ESI) m/z: $[M+4H]^{4+}/4$ calcd. for 826.2213; found, 826.8641. $[M+5H]^{5+}/5$ calcd. for 661.1786; found, 661.6305. $[M+6H]^{6+}/6$ calcd. for 551.1502; found, 551.5397. (c) Synthesis of PSGMR, HRMS (ESI) m/z: $[M+5H]^{5+}/5$ calcd. for 767.8326; found, 768.2742. $[M+6H]^{6+}/6$ calcd. for 640.0285; found, 640.3345. $[M+7H]^{7+}/7$ calcd. for 548.7398; found, 549.0886. $[M+8H]^{8+}/8$ calcd. for 480.2733; found, 480.9323.

3.4 Synthesis of PMR.

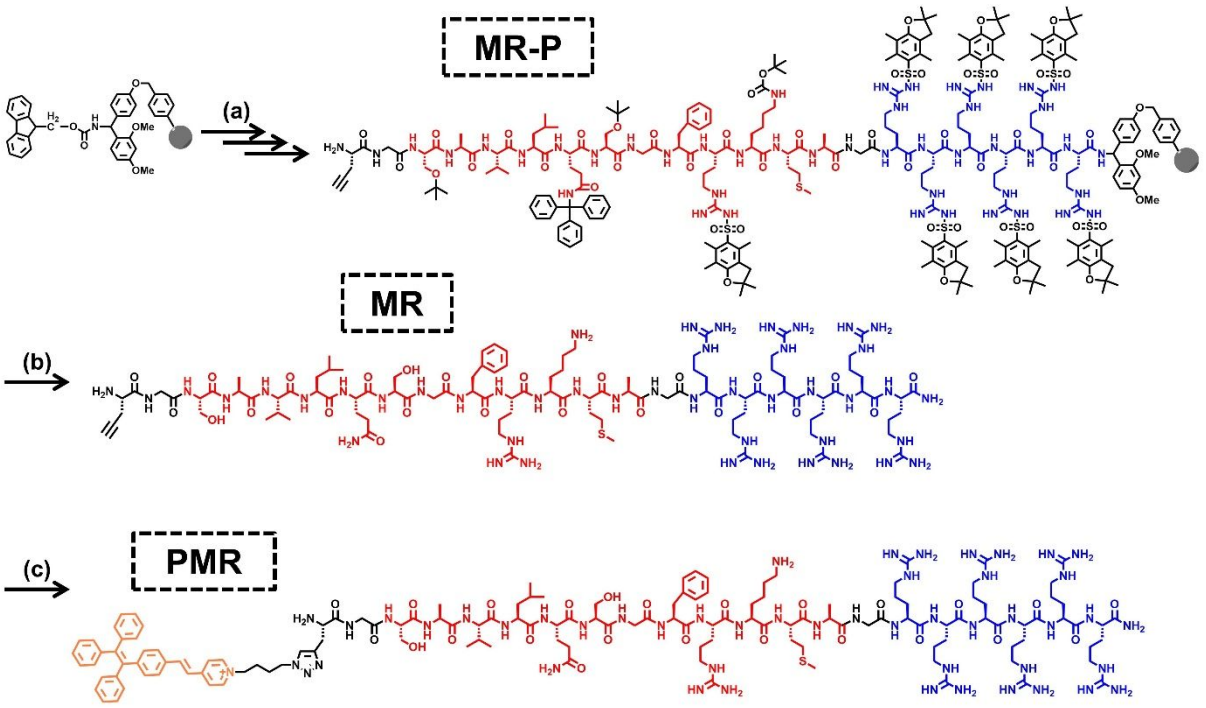

Scheme S5. The synthetic route of PMR.

The main synthetic route of PMR is three steps through standard solid phase Fmoc synthesis, thiol-maleimide Michael addition and copper-catalyzed azide-alkyne click reaction. (a) Synthesis of MR-P. (b) Synthesis of MR, HRMS (ESI) m/z: $[M+3H]^{3+}/3$ calcd. for 813.8029; found, 814.3572. $[M+4H]^{4+}/4$ calcd. for 610.5042; found, 611.1230. $[M+5H]^{5+}/5$ calcd. for 488.6849; found, 489.0517. (c) Synthesis of PMR, HRMS (ESI) m/z: $[M+4H]^{4+}/4$ calcd. for 743.9216; found, 744.3828. $[M+5H]^{5+}/5$ calcd. for 595.3388; found, 595.7583. $[M+6H]^{6+}/6$ calcd. for 496.2837; found, 496.5610. $[M+7H]^{7+}/7$ calcd. for 425.5299; found, 425.8732.

Table S1. Peptide sequences used in this study.

Peptide name	Sequences
1	CG**AVLQ/**DDD
2	**AVLQ/**FFVLKC
3	RVRR**SAVLQ/SGFRKMA**C
4	CGKLVFFG**TSAVLQ/SGFR**GDDD
MR	(Pra)G**SAVLQ/SGFRKMA**GRRRRRR
SMR	(Pra)KLVFFG**SAVLQ/SGFRKMA**RRRRRR
SGMR	(Pra)KLVFFGGG**SAVLQ/SGFRKMA**GGGRRRRRR
The bold indicates the potential M^{pro}-responsive sequence.	

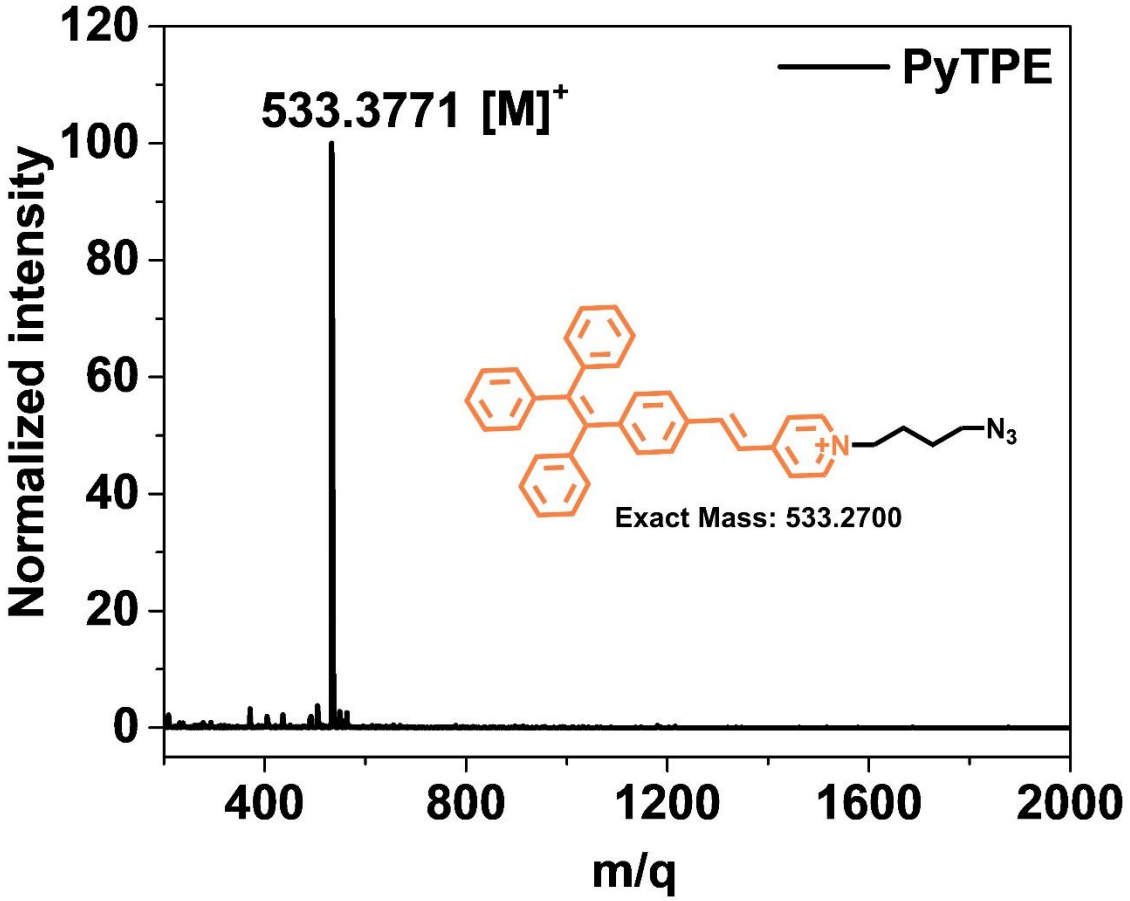

Figure S1. Electrospray ionization mass spectrometry (ESI-MS) results of PyTPE.

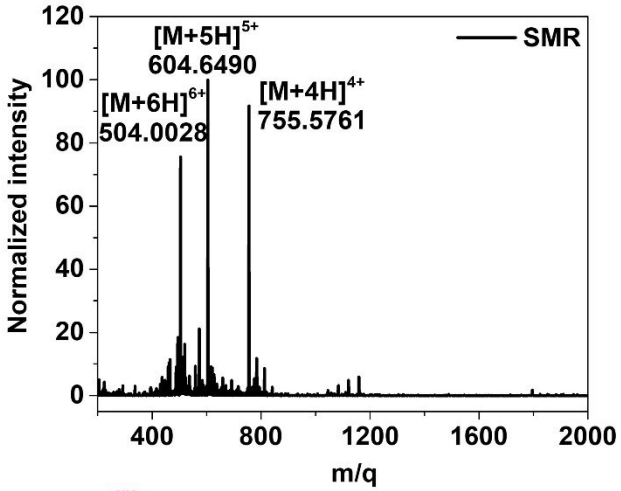

n	[M+nH]	M/q
0	3015.7518	
1	3016.7597	3016.7597
2	3017.7675	1508.8838
3	3018.7753	1006.2584
4	3019.7831	754.9458
5	3020.7910	604.1582
6	3021.7988	503.6331
Calculated data		

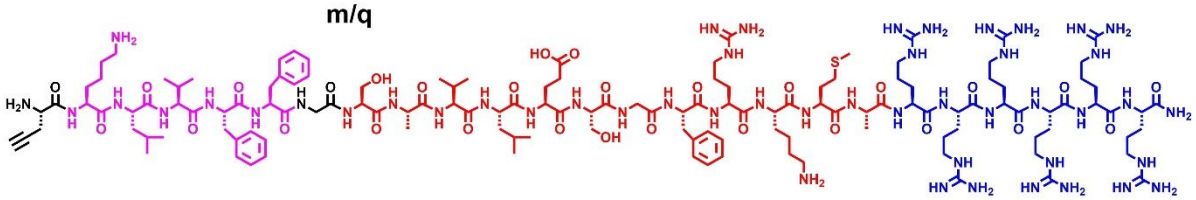

Figure S2. ESI-MS results of SMR.

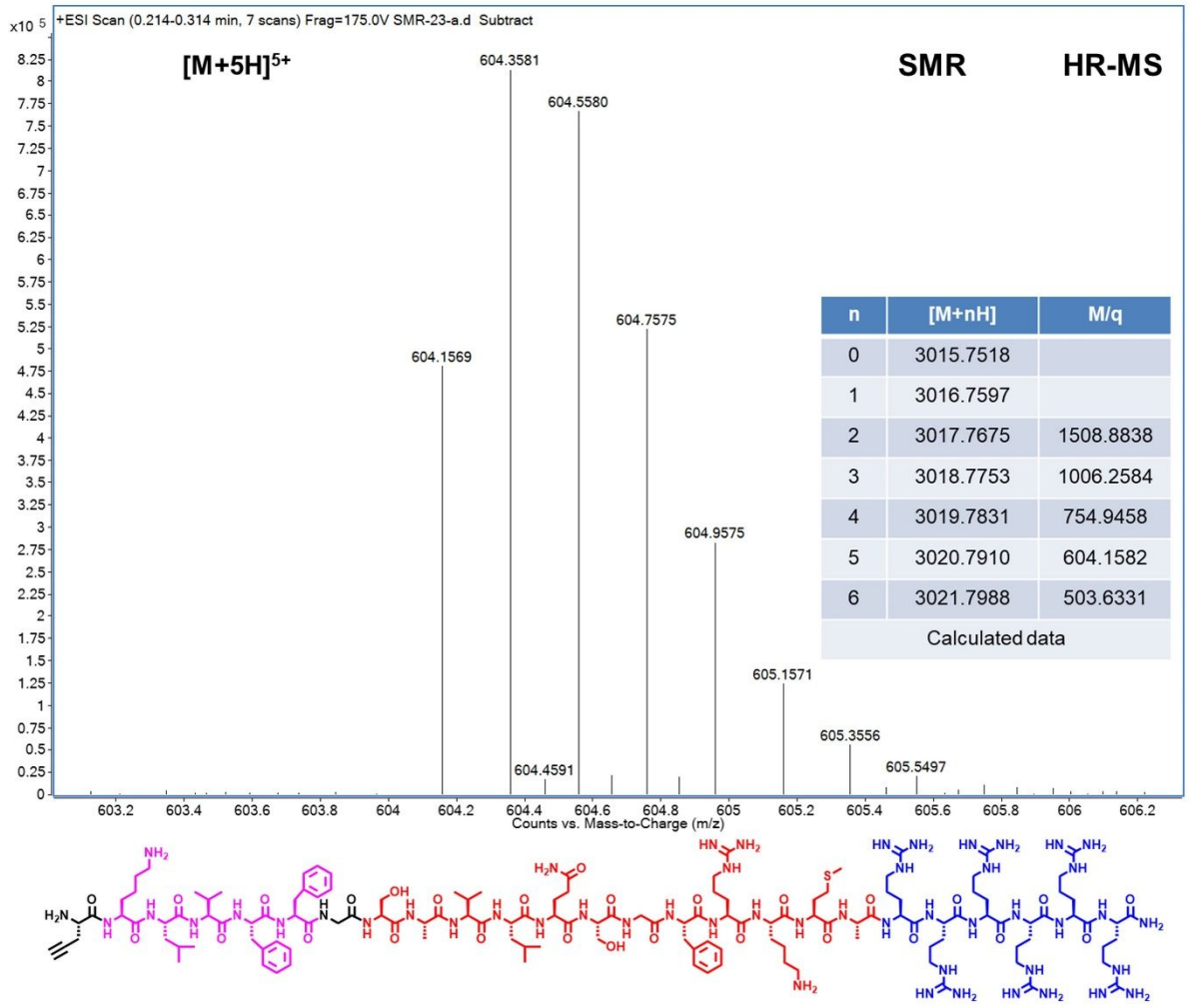

Figure S3. High resolution mass spectra (HRMS) results of SMR with five positive charges.

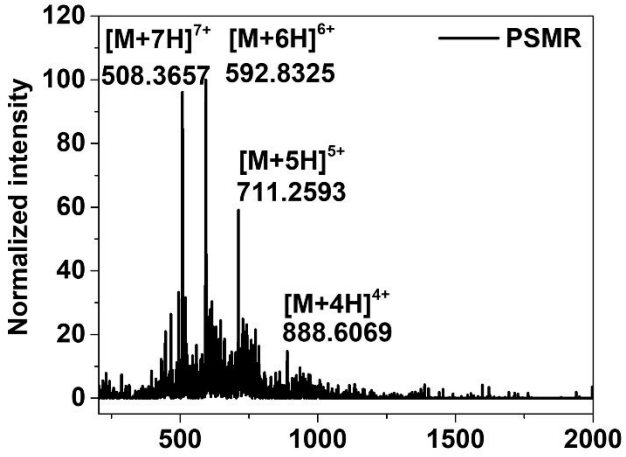

n	[M+nH]	M/q
0	3549.0218	
1	3550.0296	3550.0296
2	3551.0375	1775.5188
3	3552.0453	1184.0151
4	3553.0531	888.2633
5	3554.0609	710.8122
6	3555.0688	592.5115
7	3556.0766	508.0109
Calculated data		

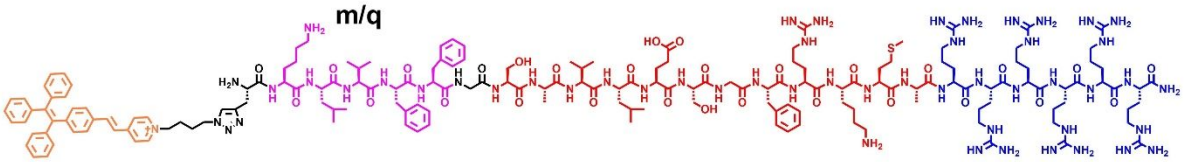

Figure S4. ESI-MS results of PSMR.

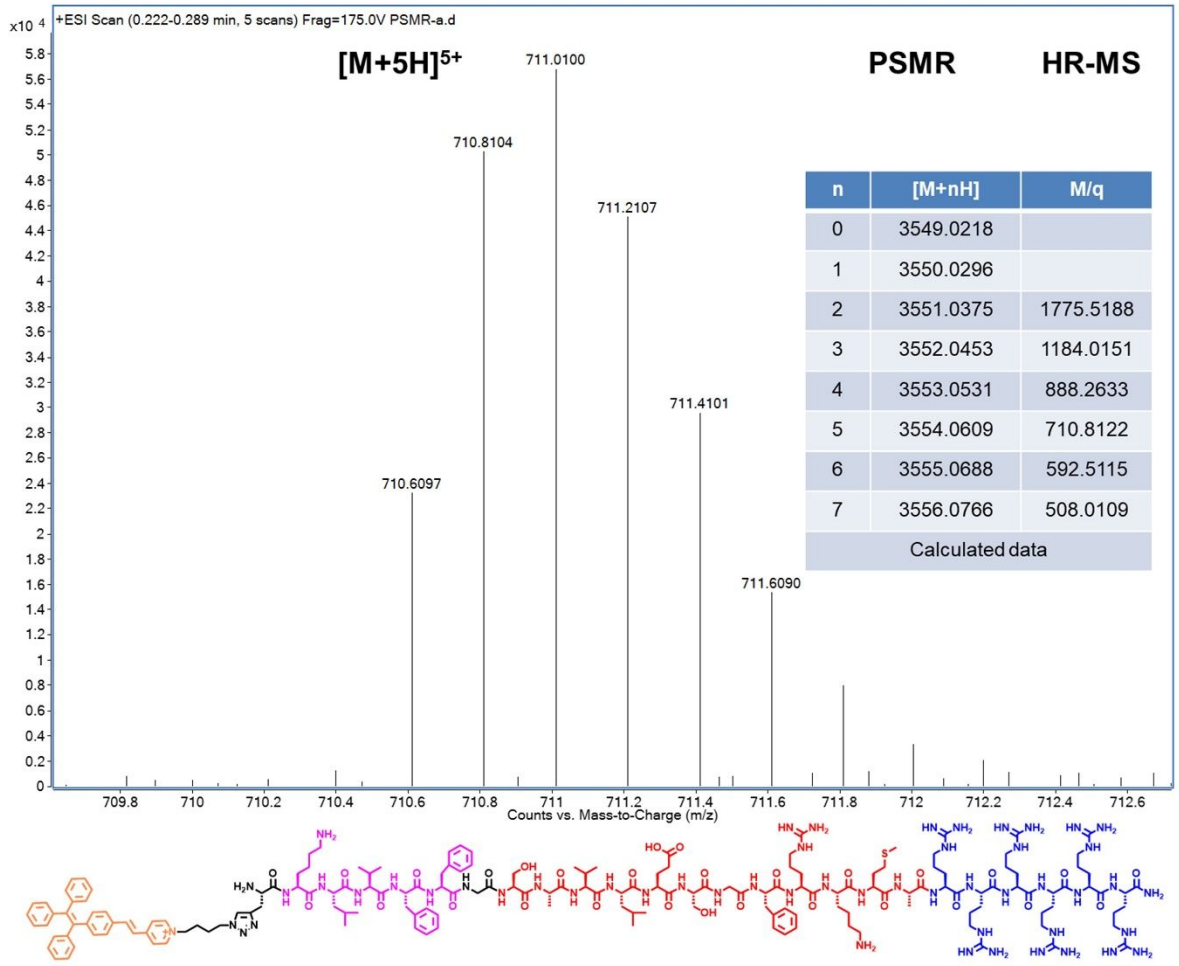

n	[M+nH]	M/q
0	3549.0218	
1	3550.0296	
2	3551.0375	1775.5188
3	3552.0453	1184.0151
4	3553.0531	888.2633
5	3554.0609	710.8122
6	3555.0688	592.5115
7	3556.0766	508.0109
Calculated data		

Figure S5. HRMS results of PSMR with five positive charges.

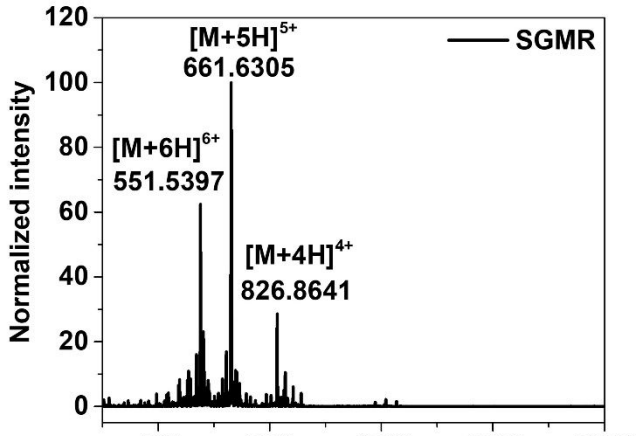

n	[M+nH]	M/q
0	3300.8541	
1	3301.8619	3301.8619
2	3302.8697	1651.4349
3	3303.8775	1101.2925
4	3304.8853	826.2213
5	3305.8931	661.1786
6	3306.9009	551.1502
Calculated data		

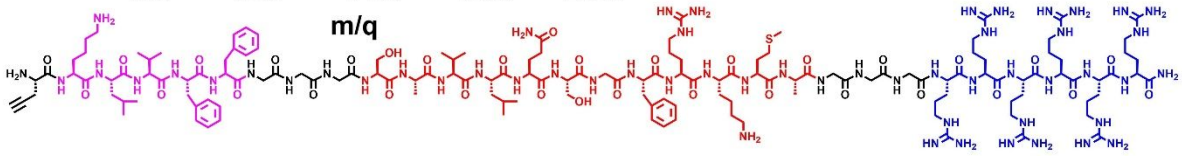

Figure S6. ESI-MS results of SGMR.

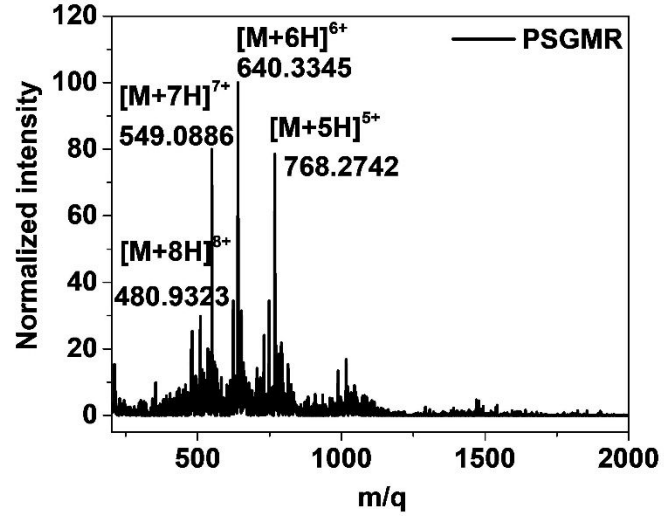

n	[M+nH]	M/q
0	3834.1239	
1	3835.1317	3835.1317
2	3836.1395	1918.0698
3	3837.1473	1279.0491
4	3838.1551	959.5388
5	3839.1629	767.8326
6	3840.1707	640.0285
7	3841.1785	548.7398
8	3842.1863	480.2733
Calculated data		

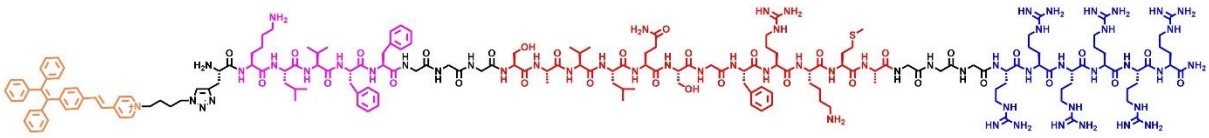

Figure S7. ESI-MS results of PSGMR.

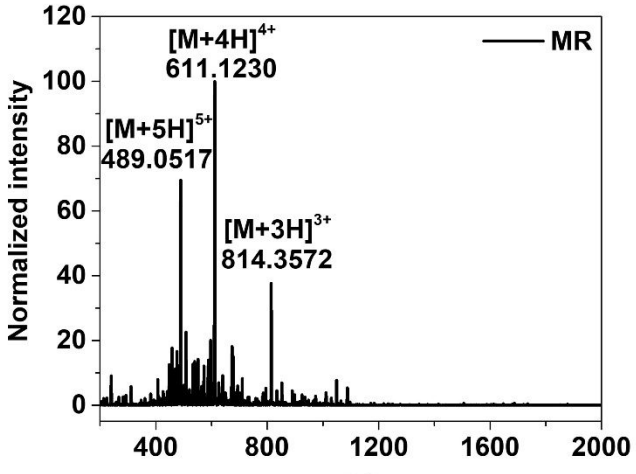

n	[M+nH]	M/q
0	2438.3854	
1	2439.3932	2439.3932
2	2440.1010	1220.2005
3	2441.4088	813.8029
4	2442.4166	610.5042
5	2443.4244	488.6849
Calculated data		

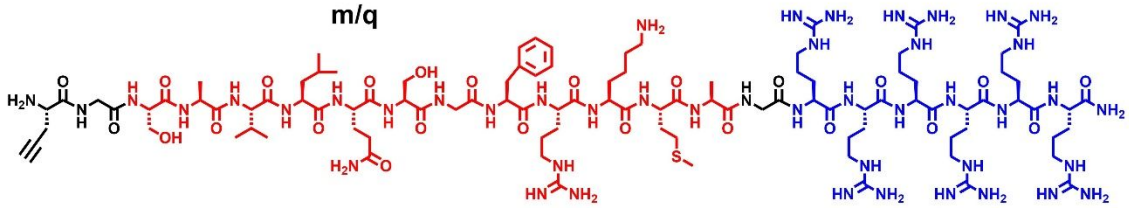

Figure S8. ESI-MS results of MR.

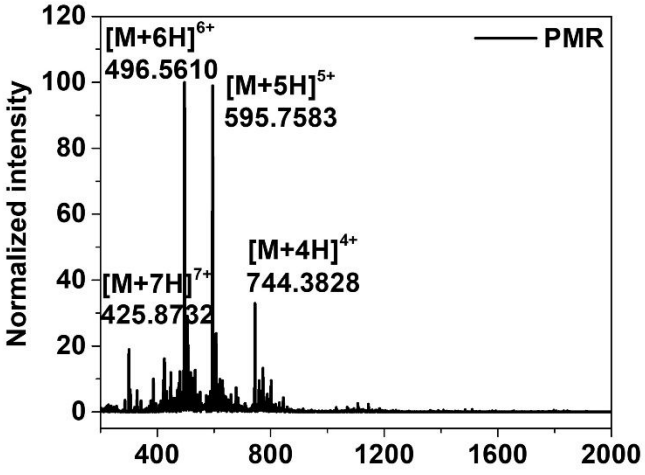

n	[M+nH]	M/q
0	2971.6552	
1	2972.6630	2972.6630
2	2973.6708	1486.8354
3	2974.6786	991.5595
4	2975.6864	743.9216
5	2976.6942	595.3388
6	2977.7020	496.2837
7	2978.7098	425.5299
Calculated data		

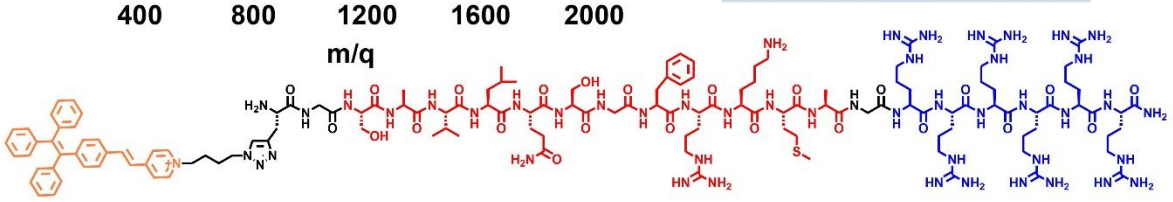

Figure S9. ESI-MS results of PMR.

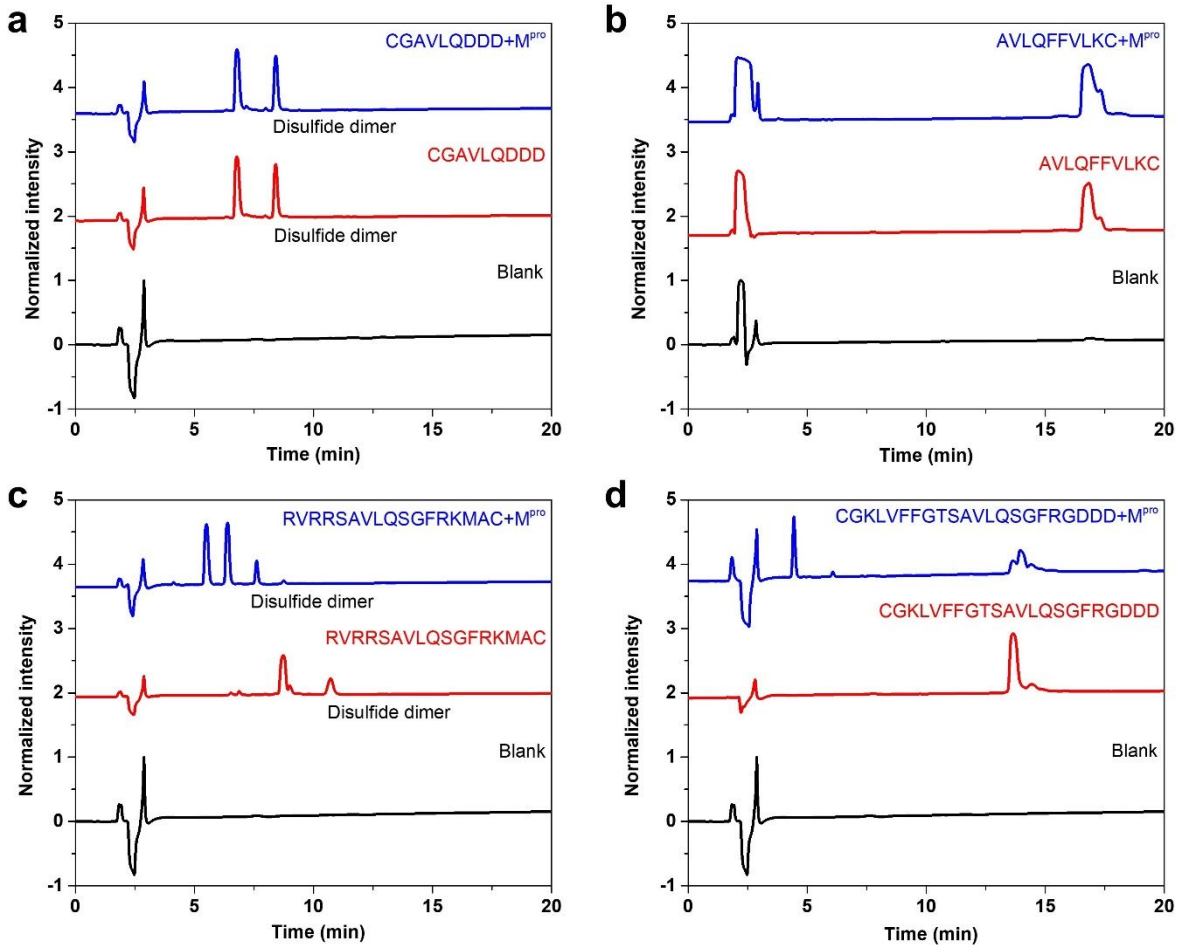

Figure S10. HPLC results of different peptides before and after incubation with M^{pro} showing that some AVLQ peptide sequence cannot be cleaved by M^{pro}. (a) CGAVLQDDD was not cleaved by M^{pro}. (b) AVLQFFVLKC was not cleaved by M^{pro}. (c) RVRRSAVLQSGFRKMAC was cleaved by M^{pro}. (d) CGKLVFFGTSAVLQSGFRGDDD was cleaved by M^{pro}.

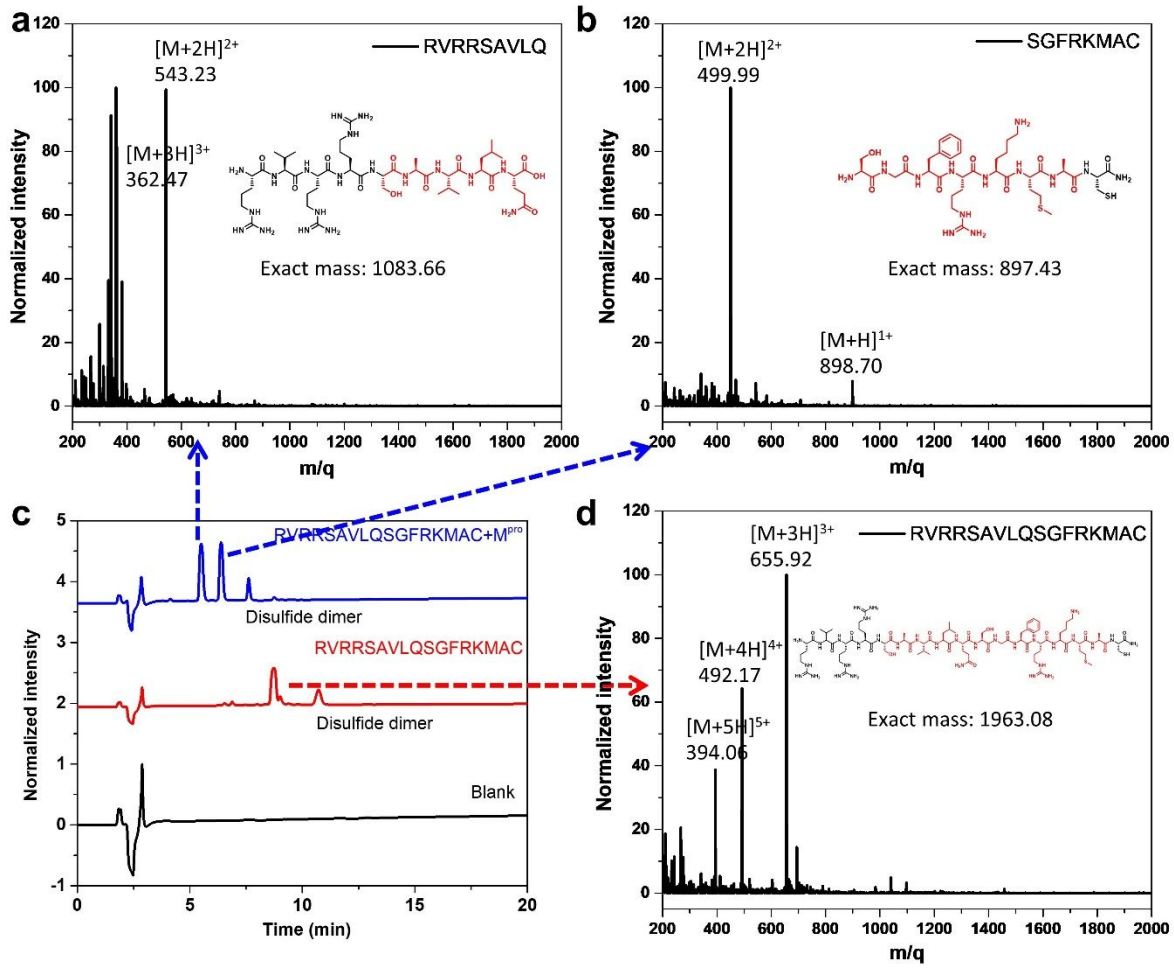

Figure S11. HPLC and ESI-MS results of compound RVRRSAVLQSGFRKMAC before and after incubation with M^{pro} showing that RVRRSAVLQSGFRKMAC can be cleaved by M^{pro} after AVLQ. (a) ESI-MS results of RVRRSAVLQ. (b) ESI-MS results of SGFRKMAC. (c) HPLC results of RVRRSAVLQSGFRKMAC before and after incubation with M^{pro}. (d) ESI-MS results of RVRRSAVLQSGFRKMAC.

vials containing the respective solutions under UV light (365 nm, 16 W)

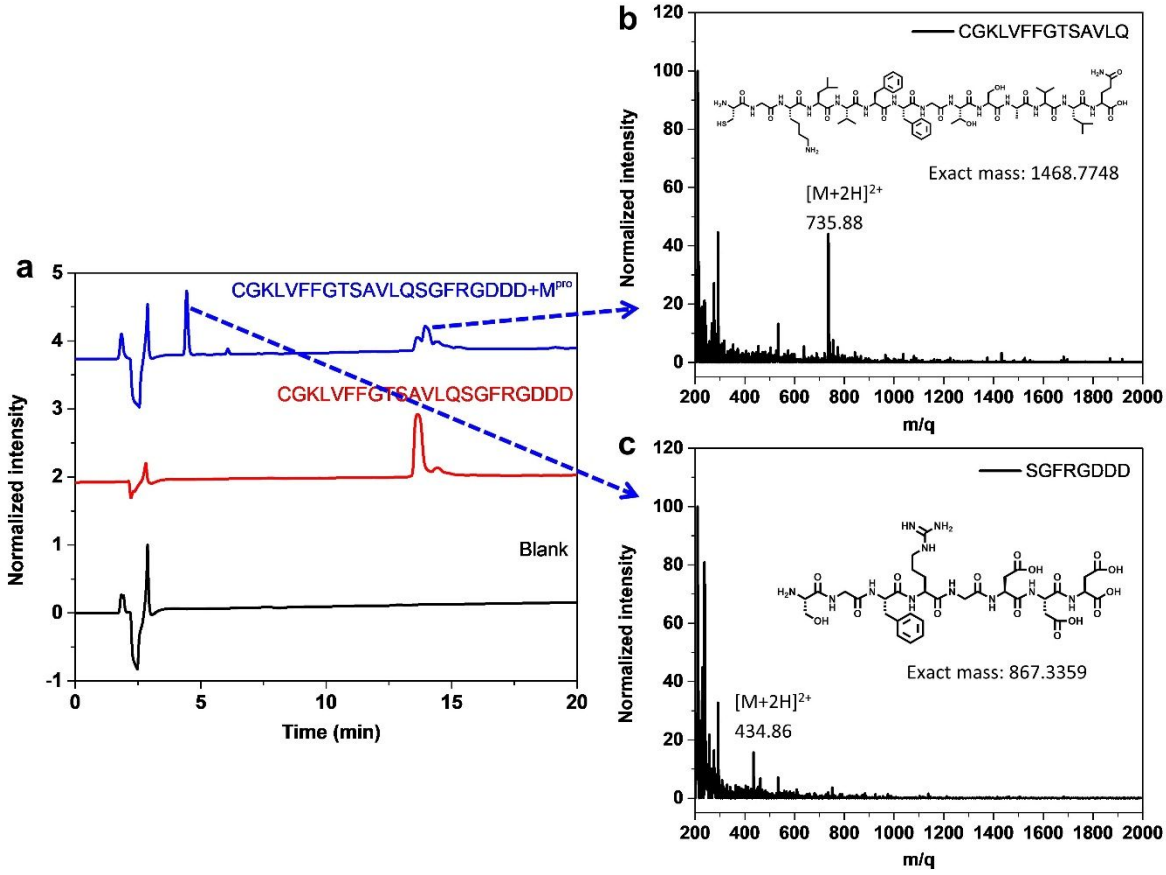

Figure S12. HPLC and ESI-MS results of compound CGKLVFFGTSAVLQSGFRGDDD before and after incubation with M^{pro} showing that CGKLVFFGTSAVLQSGFRGDDD can be cleaved by M^{pro} after AVLQ. (a) HPLC results of CGKLVFFGTSAVLQSGFRGDDD before and after incubation with M^{pro}. (b) ESI-MS results of CGKLVFFGTSAVLQ. (c) ESI-MS results of SGFRGDDD.

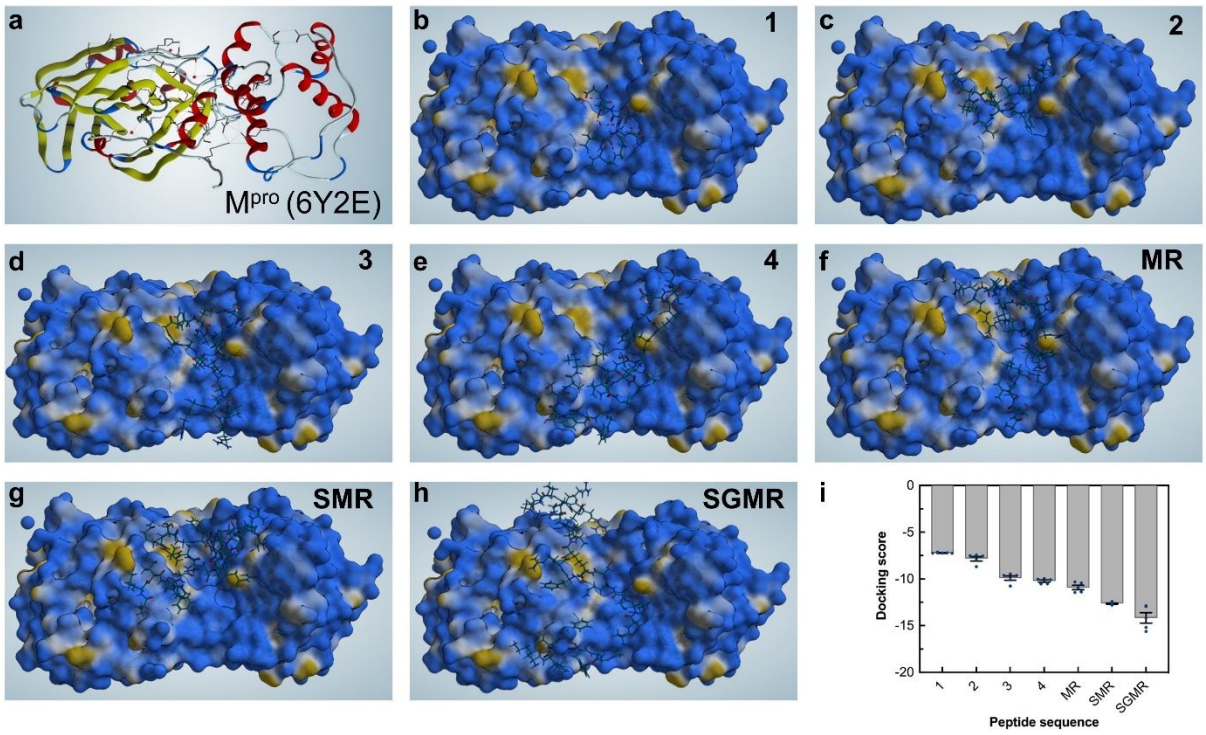

Figure S13. Molecular docking and theoretical calculation results of SARS-CoV-2 M^{pro} (PDB code 6Y2E) in complex with the seven different peptides through a Molecular Operating Environment (MOE) software. (a) M^{pro} 3D structure. (b) M^{pro} with CGAVLQDDD (**1**). (c) M^{pro} with AVLQFFVLKC (**2**). (d) M^{pro} with RVRRSAVLQSGFRKMAC (**3**). (e) M^{pro} with CGKLVFFGTSAVLQ/SGFRGDDD (**4**). (f) M^{pro} with (Pra)GSAVLQ/SGFRKMAGRRRRRR (**MR**). (g) M^{pro} with (Pra)KLVFFGSAVLQ/SGFRKMARRRRRR (**SMR**). (h) M^{pro} with (Pra)KLVFFGGGSAVLQ/SGFRKMAGGGRRRRRR (**SGMR**). The blue, yellow, and white represent hydrophilic, lipophilic, and neutral part of peptide in the M^{pro}. (i) The docking scores of M^{pro} with different peptides showing their enhanced binding abilities.

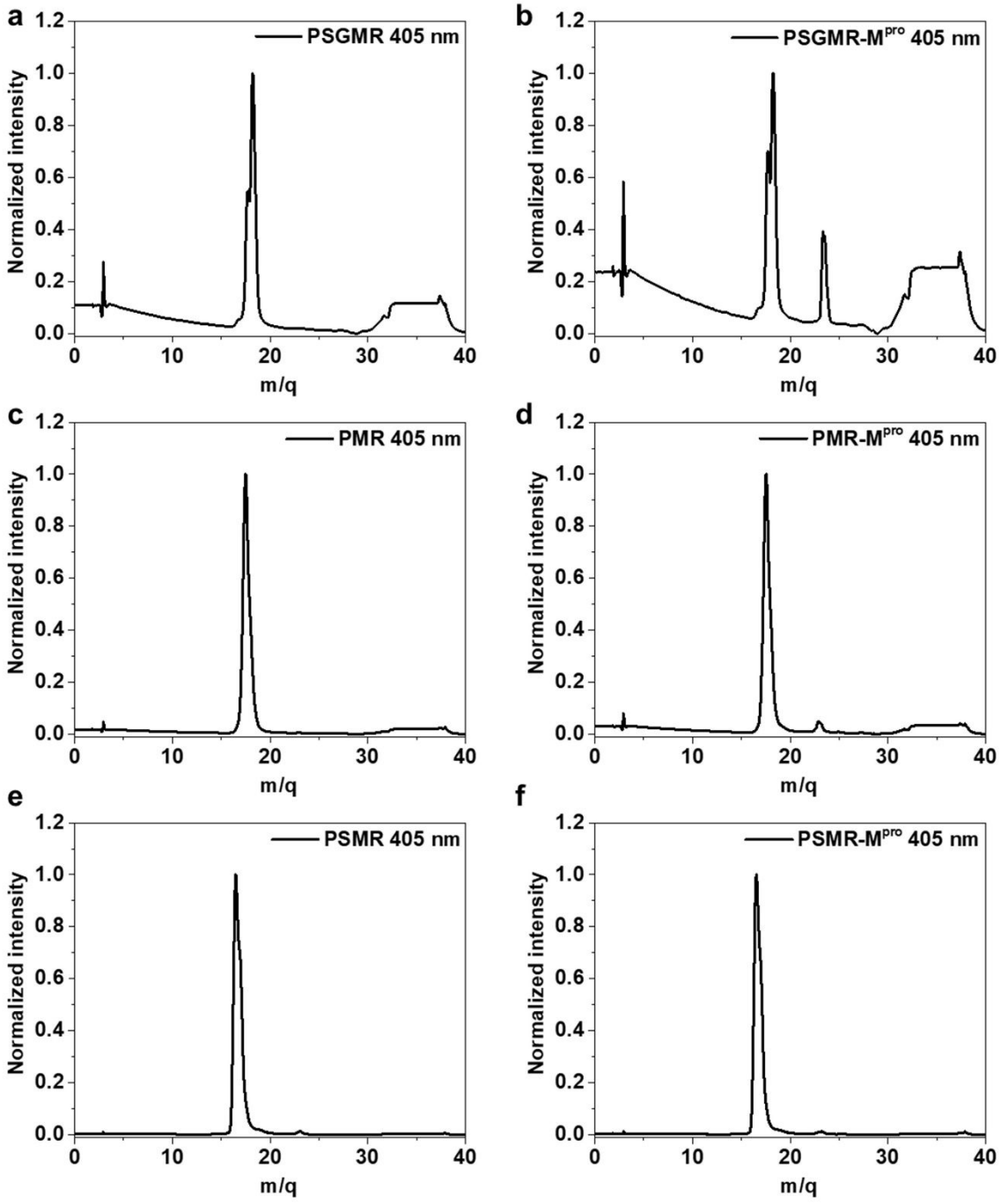

Figure S14. HPLC results of compounds PSGMR, PMR, and PSMR before and after incubation with M^{pro} for 1 h showing that PSGMR and PMR not PSMR can be cleaved by M^{pro}. (a-b) PSGMR. (c-d) PMR. (e-f) PSMR.

a

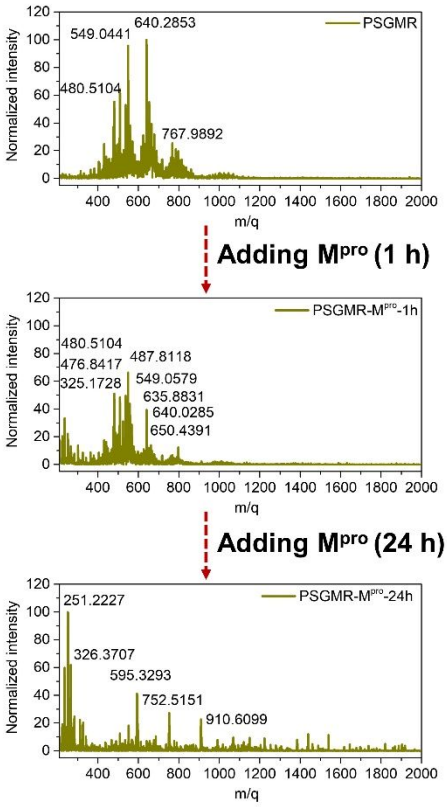

b

Before M^{pro} cleavage

n	[M+nH]	M/q
0	3834.1239	
1	3835.1317	3835.1317
2	3836.1395	1918.0698
3	3837.1473	1279.0491
4	3838.1551	959.5388
5	3839.1629	767.8326
6	3840.1707	640.0285
7	3841.1785	548.7398
8	3842.1863	480.2733

Calculated data (PSGMR)

After M^{pro} cleavage

n	[M+nH]	M/q
0	1950.0439	
1	1951.0517	1951.0517
2	1952.0595	976.0298
3	1953.0673	651.0224
4	1954.0751	488.5188
5	1955.0829	391.0166
6	1956.0907	326.0151

Calculated data (PSG)

n	[M+nH]	M/q
0	1902.0905	
1	1903.0983	1951.0517
2	1904.1061	952.0531
3	1905.1139	635.0380
4	1906.1217	476.5304
5	1907.1295	381.4259
6	1908.1373	318.0229

Calculated data (MR)

Figure S15. ESI-MS results of PSGMR before and after incubation with M^{pro} for 1 h and 24 h showing that PSGMR can be cleaved by M^{pro}. (a) ESI-MS. (b) The calculated data. The red dotted box includes the target molecular weight found.

a

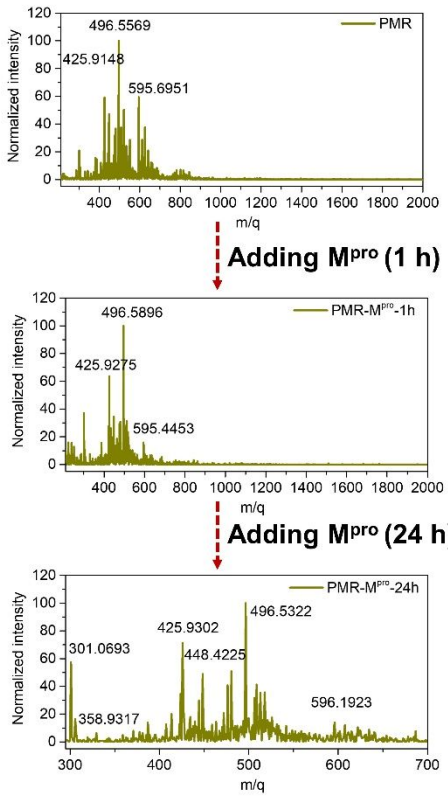

b

Before M^{pro} cleavage

n	[M+nH]	M/q
0	2971.6552	
1	2972.6630	2972.6630
2	2973.6708	1486.8354
3	2974.6786	991.5595
4	2975.6864	743.9216
5	2976.6942	595.3388
6	2977.7020	496.2837
7	2978.7098	425.5299
8	2979.7176	372.4647

Calculated data (PMR)

After M^{pro} cleavage

n	[M+nH]	M/q
0	1201.6180	
1	1202.6258	1202.6258
2	1203.6336	601.8168
3	1204.6414	401.5471
4	1205.6492	301.4123
5	1206.6570	241.3314
6	1207.6648	201.2775

Calculated data (PM)

n	[M+nH]	M/q
0	1788.0477	
1	1789.0555	1789.0555
2	1790.0633	895.0317
3	1791.0711	597.0237
4	1792.0789	448.0197
5	1793.0867	358.6173
6	1794.0945	299.0158

Calculated data (MR)

Figure S16. ESI-MS results of PMR before and after incubation with M^{pro} for 1 h and 24 h showing that PMR can be cleaved by M^{pro}. (a) ESI-MS. (b) The calculated data. The red dotted box includes the target molecular weight found.

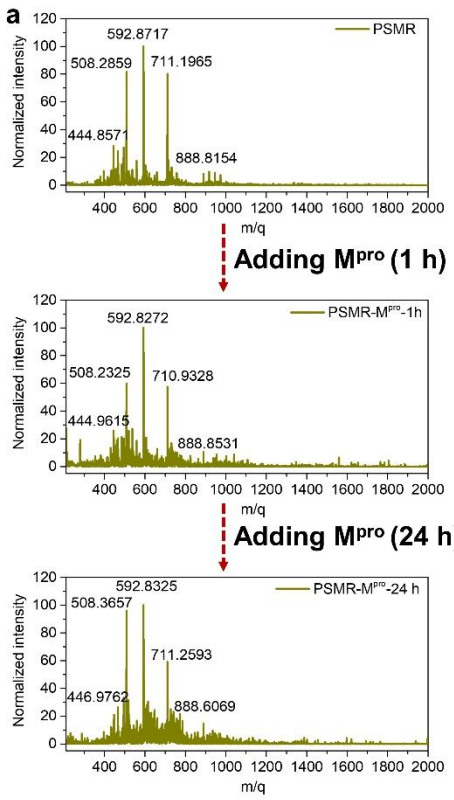

b

Before M^{pro} cleavage

n	[M+nH]	M/q
0	3549.0218	
1	3550.0296	3550.0296
2	3551.0375	1775.5188
3	3552.0453	1184.0151
4	3553.0531	888.2633
5	3554.0609	710.8122
6	3555.0688	592.5115
7	3556.0766	508.0109
8	3557.0844	444.6356

Calculated data (PSMR)

After M^{pro} cleavage

n	[M+nH]	M/q
0	1836.0036	
1	1837.0114	1837.0114
2	1838.0192	919.0096
3	1839.0271	613.0090
4	1840.0349	460.0087
5	1841.0427	368.2085
6	1842.0505	307.0084

Calculated data (PS)

n	[M+nH]	M/q
0	1731.0263	
1	1732.0341	1732.0341
2	1733.0419	866.5210
3	1734.0497	578.0166
4	1735.0575	433.7644
5	1736.0653	347.2131
6	1737.0731	289.5122

Calculated data (MR)

Figure S17. ESI-MS results of PSMR before and after incubation with M^{pro} for 1 h and 24 h showing that PSMR can be cleaved by M^{pro}. (a) ESI-MS. (b) The calculated data. The red dotted box includes the target molecular weight found.

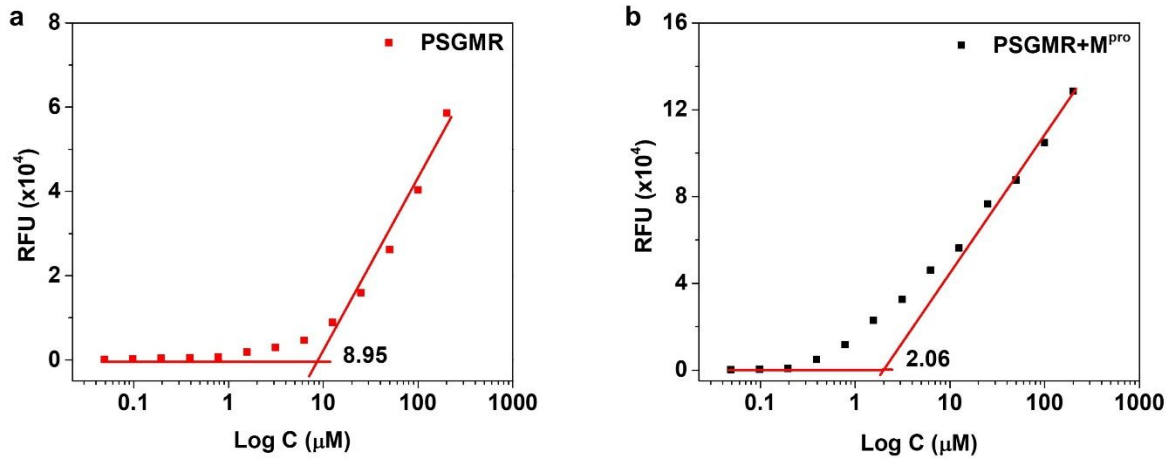

Figure S18. The Critical micelle concentrations (CMC) value of PSGMR and PSGMR after incubation with 200 nM M^{pro}. The fluorescence intensity of PyTPE was analyzed as a function of the PSGMR concentration (λ_{Ex} = 405 nm, λ_{Em} = 590 nm).[6]

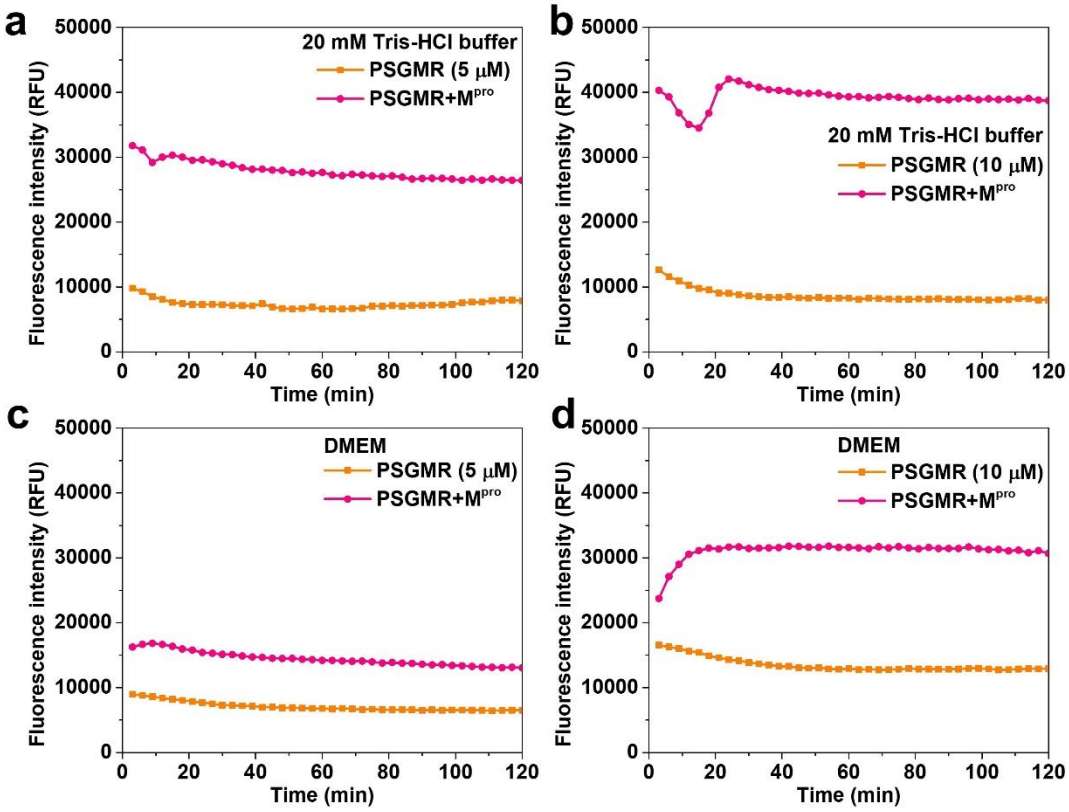

Figure S19. Time-dependent fluorescence spectra of (a, c) 5 μM and (b, d) 10 μM PSGMR incubation with M^{pro} in 20 mM Tris-HCl buffer and DMEM showing that high concentrations of PSGMR can aggregate easily with strong fluorescence both in 20 mM Tris-HCl buffer and DMEM.

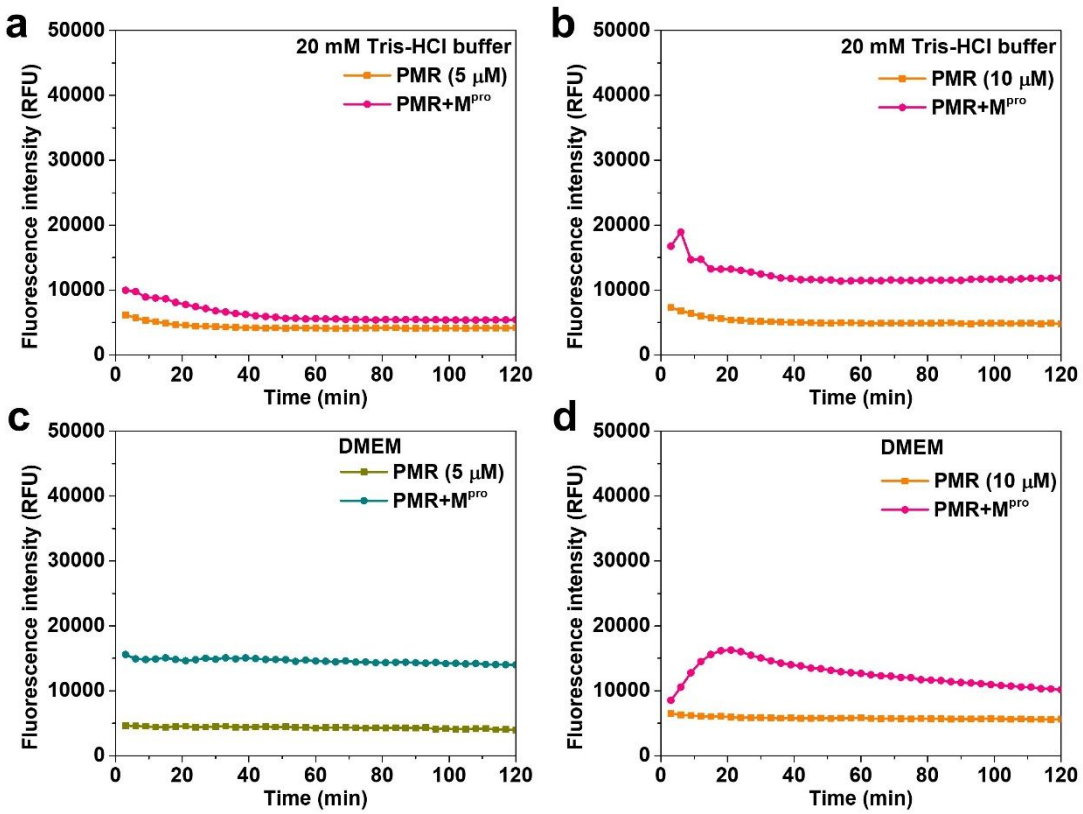

Figure S20. Time-dependent fluorescence spectra of (a, c) 5 μM and (b, d) 10 μM PMR incubation with M^{pro} in 20 mM Tris-HCl buffer and DMEM showing that high concentrations of PMR can easily aggregate with strong fluorescence both in 20 mM Tris-HCl buffer and DMEM.

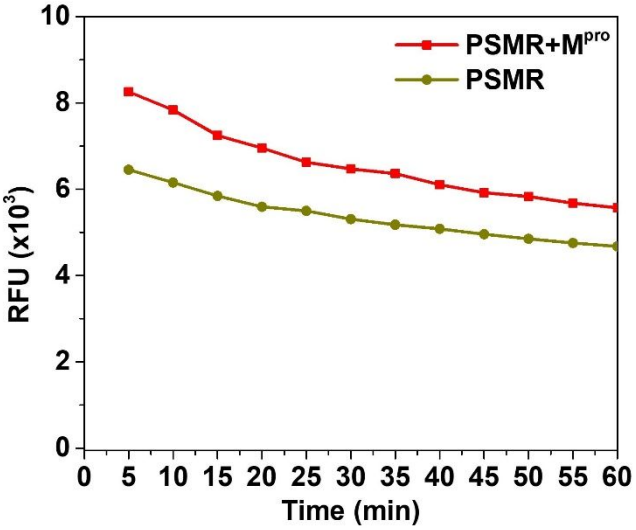

Figure S21. Time-dependent fluorescence spectra of 10 μM PSMR incubation with M^{pro} in 20 mM Tris-HCl buffer showing that PSMR cannot aggregate with weak fluorescence in 20 mM Tris-HCl buffer.

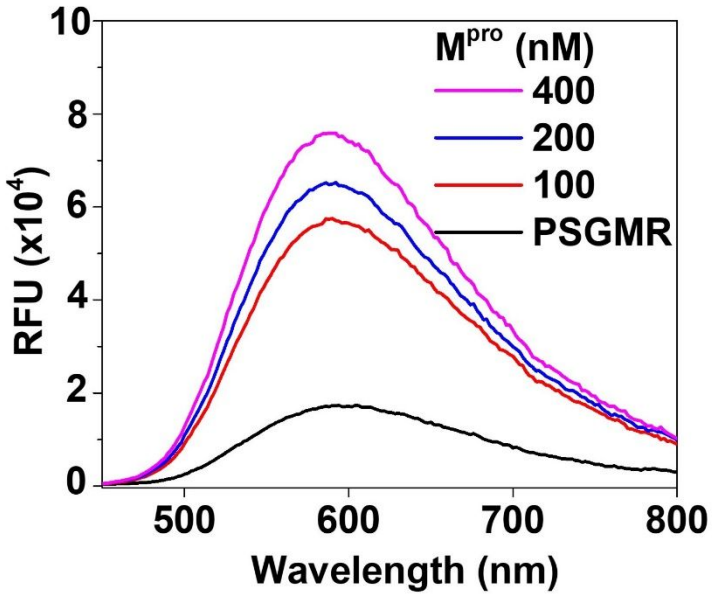

Figure S22. Fluorescence spectra of PSGMR with different concentration of M^{pro} showed the fluorescence increase because of M^{pro}.

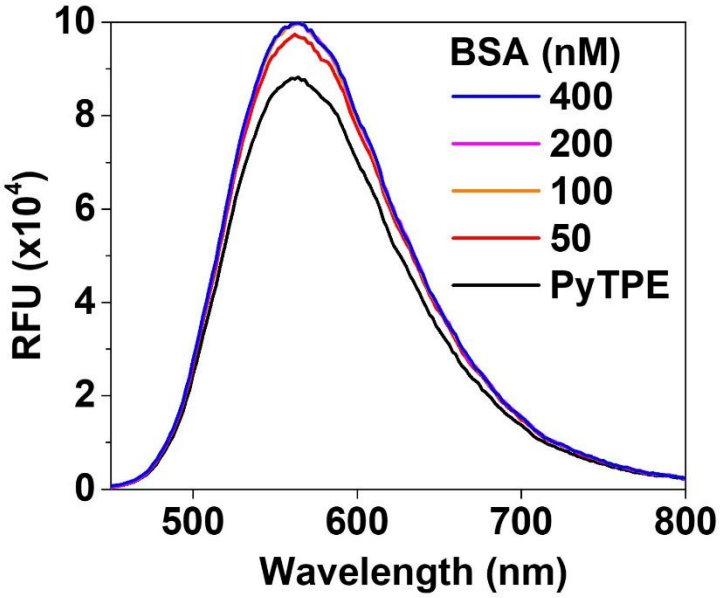

Figure S23. Fluorescence spectra of PyTPE with different concentration of BSA showed the fluorescence increase because of electrostatic interaction.

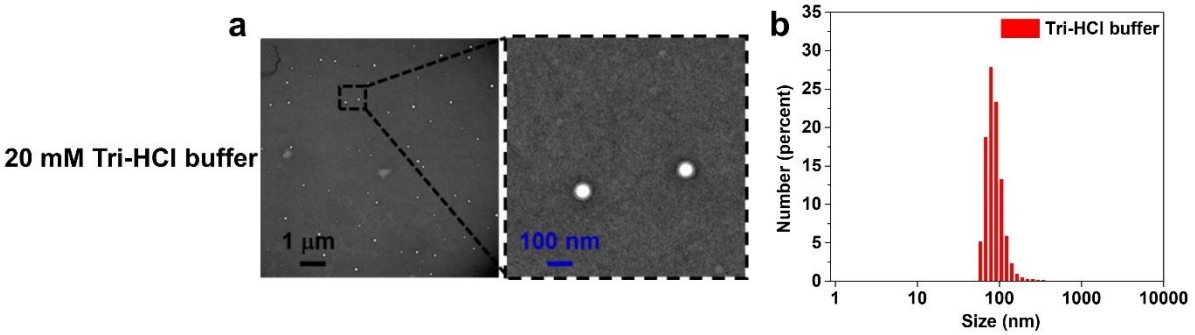

Figure S24. (a) Transmission electron microscope (TEM) images and (b) hydrodynamic size of 20 mM Tris-HCl buffer.

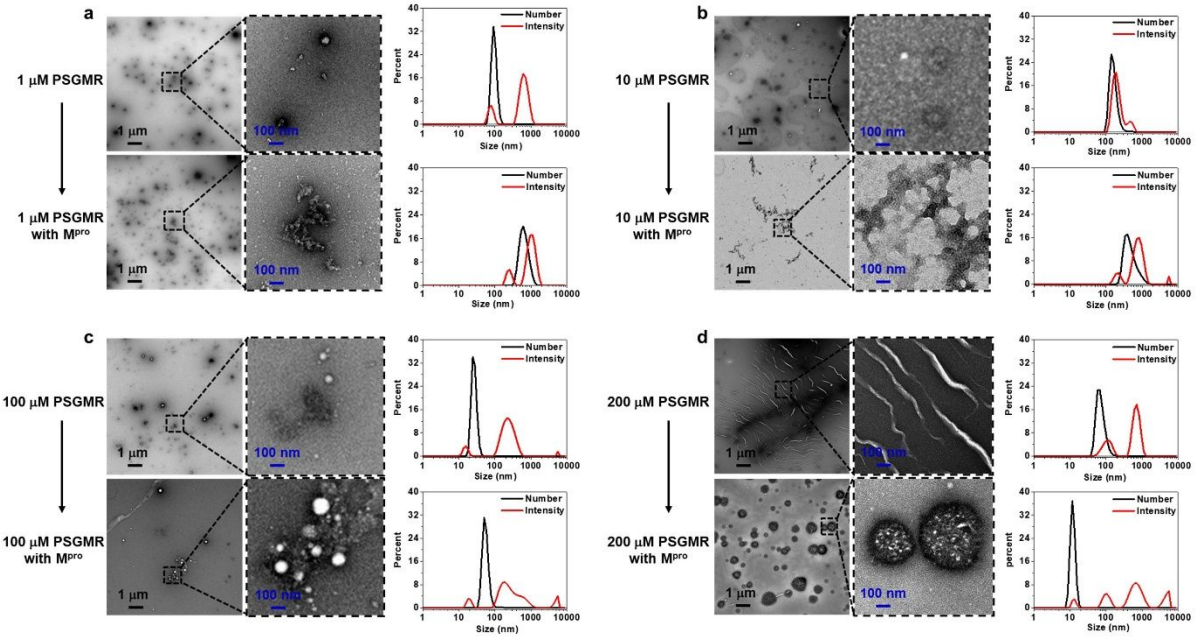

Figure S25. (a) Transmission electron microscope (TEM) images and (b) hydrodynamic sizes of 1 μM, 10 μM, 100 μM, and 200 μM PSGMR incubated with and without M^{pro} in 20 mM Tris-HCl buffer.

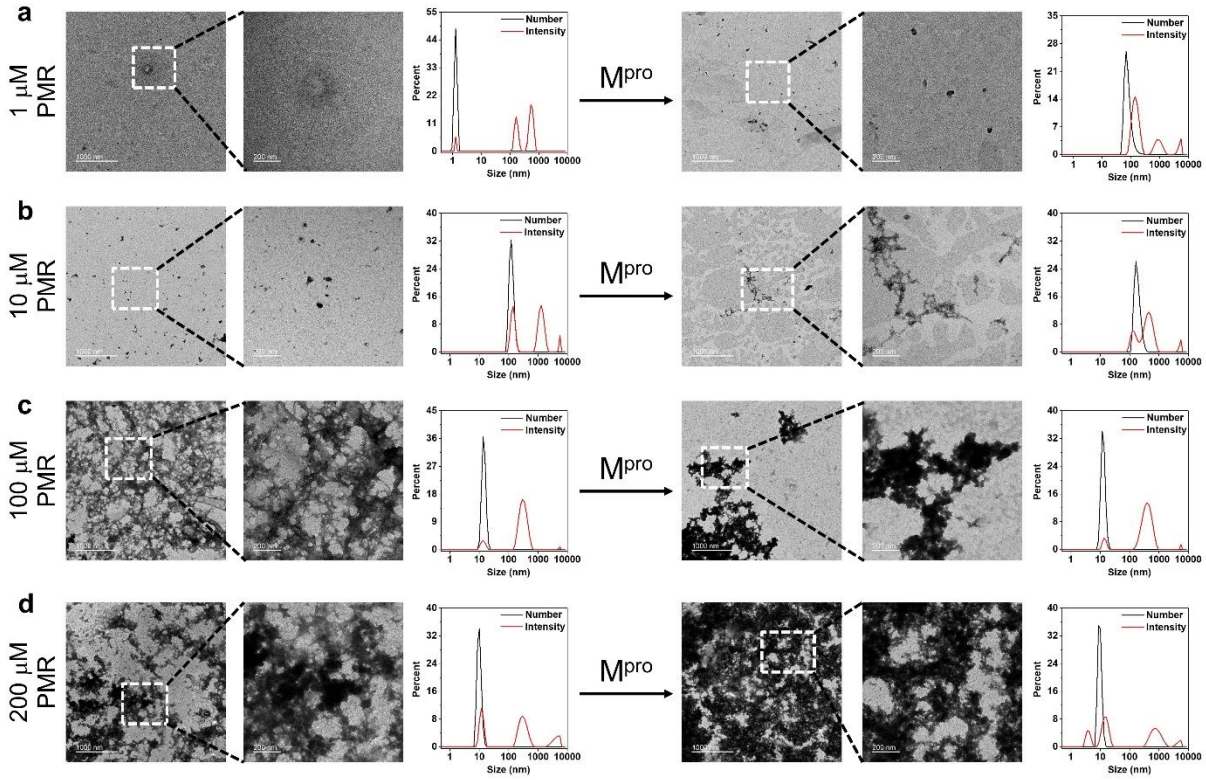

Figure S26. (a) Transmission electron microscope (TEM) images and (b) hydrodynamic sizes of 1 μM, 10 μM, 100 μM, and 200 μM PMR incubated with and without M^{pro} in 20 mM Tris-HCl buffer.

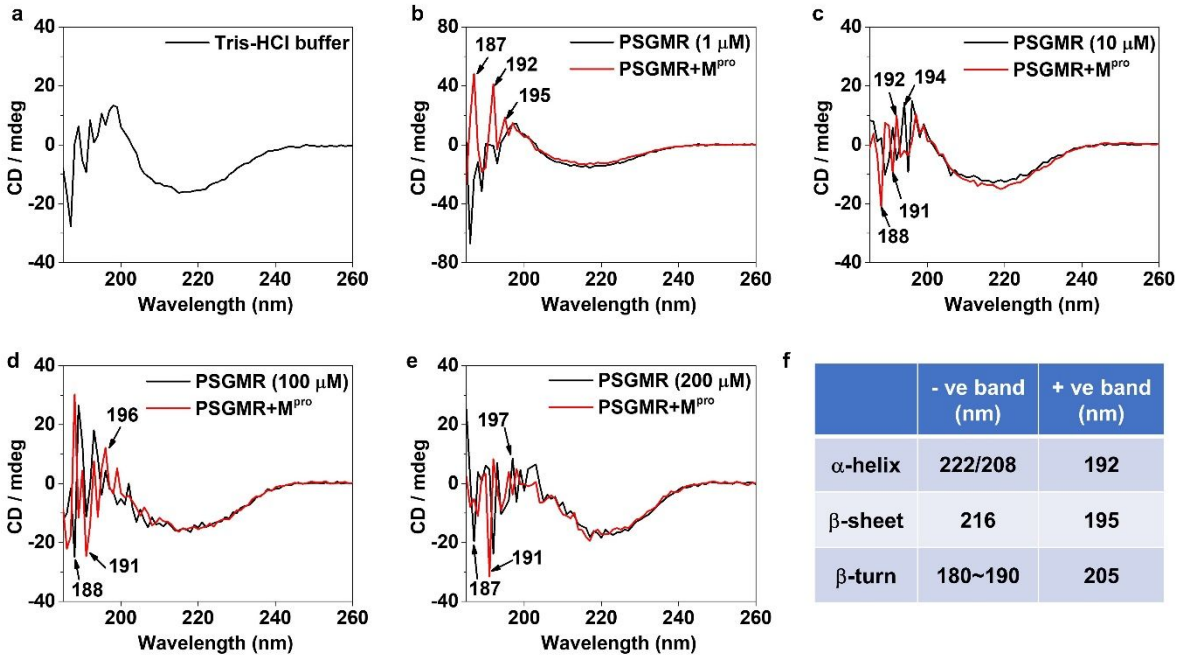

f

	- ve band (nm)	+ ve band (nm)
α-helix	222/208	192
β-sheet	216	195
β-turn	180~190	205

Figure S27. Circular dichroism (CD) spectra of (a) 20 mM Tris-HCl buffer and (b) 1 μM, (c) 10 μM, (d) 100 μM, and (e) 200 μM PSGMR before and after incubation with 200 nM M^{pro}. (f) the peak values of α-helix, β-sheet, and β-turn structures in a protein molecule indicated by CD spectroscopy.

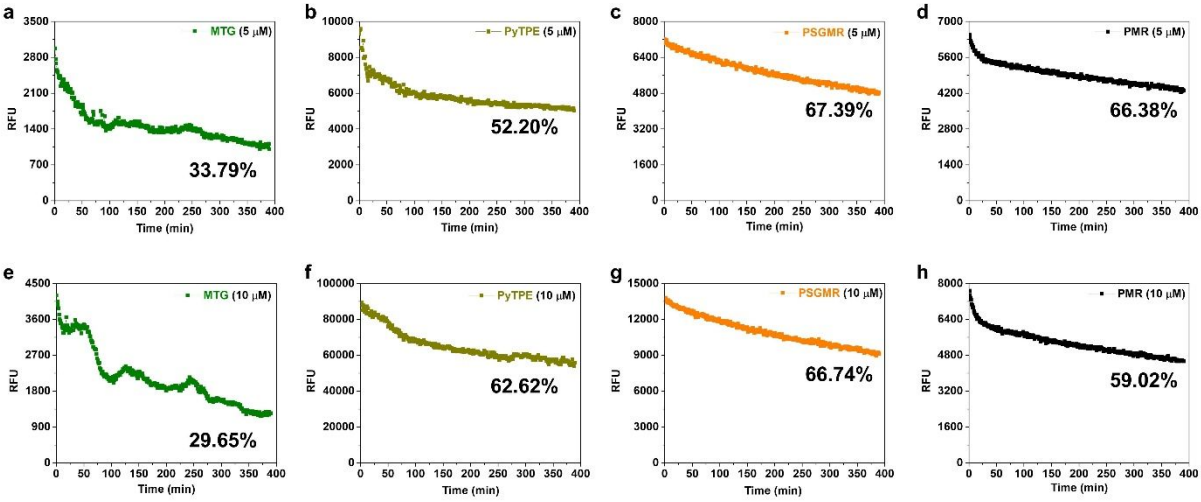

Figure S28. Photostability assay and relative remaining fluorescence intensity of different concentrations of a commercial dye Mito tracker green (MTG), PyTPE, PSGMR, and PMR after 6.5 h continuous scanning (scan every one minute), suggesting good photostability of AIEgens.

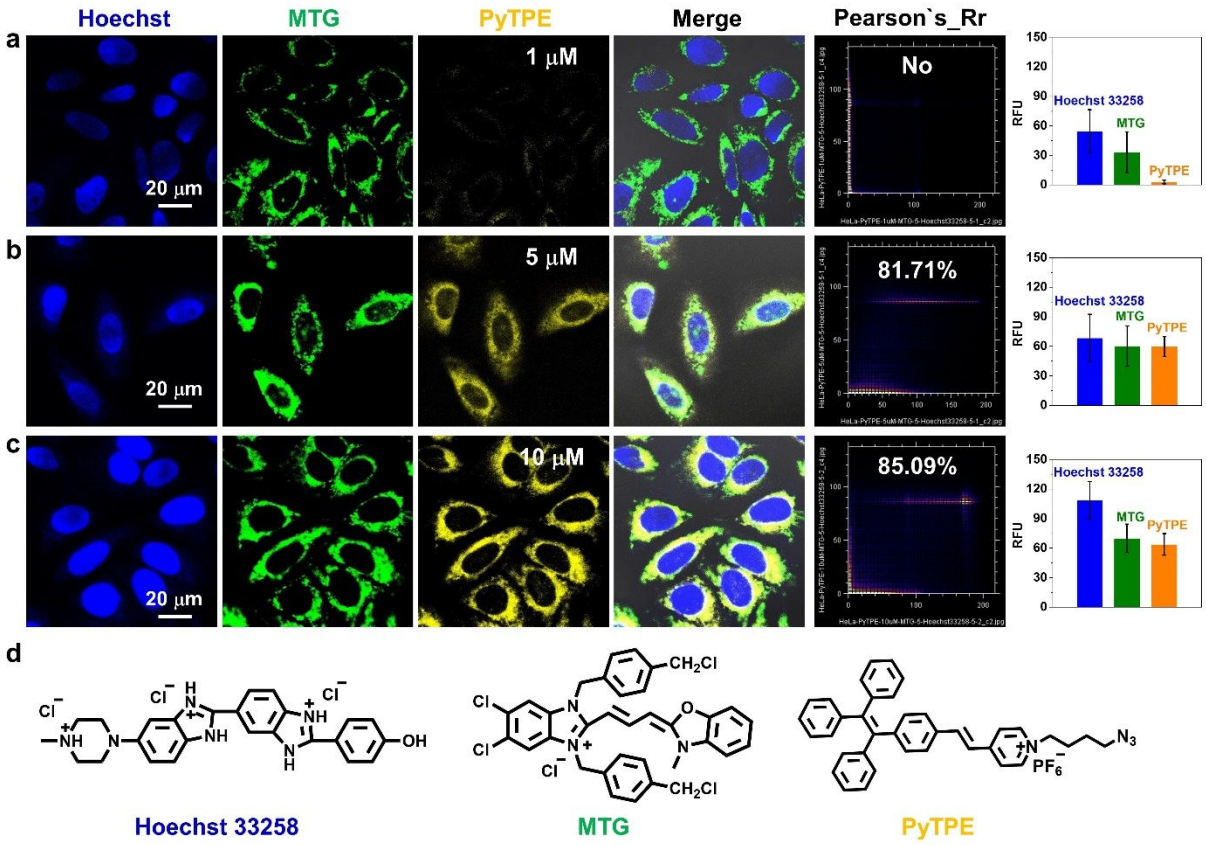

Figure S29. Confocal laser scanning microscopy (CLSM) images of Hela cells incubated with Hoechst 33258, MTG, and PyTPE. The cell images, Pearson correlation coefficient of co-localization and the average fluorescence intensities of HeLa cells incubated with (a) 1 μM, (b) 5 μM, and (c) 10 μM PyTPE as well as 5 μM Hoechst 33258, and 1 μM MTG for 3 h. (d) The chemical formula of Hoechst 33258, MTG and PyTPE. Scale bar = 20 μm.

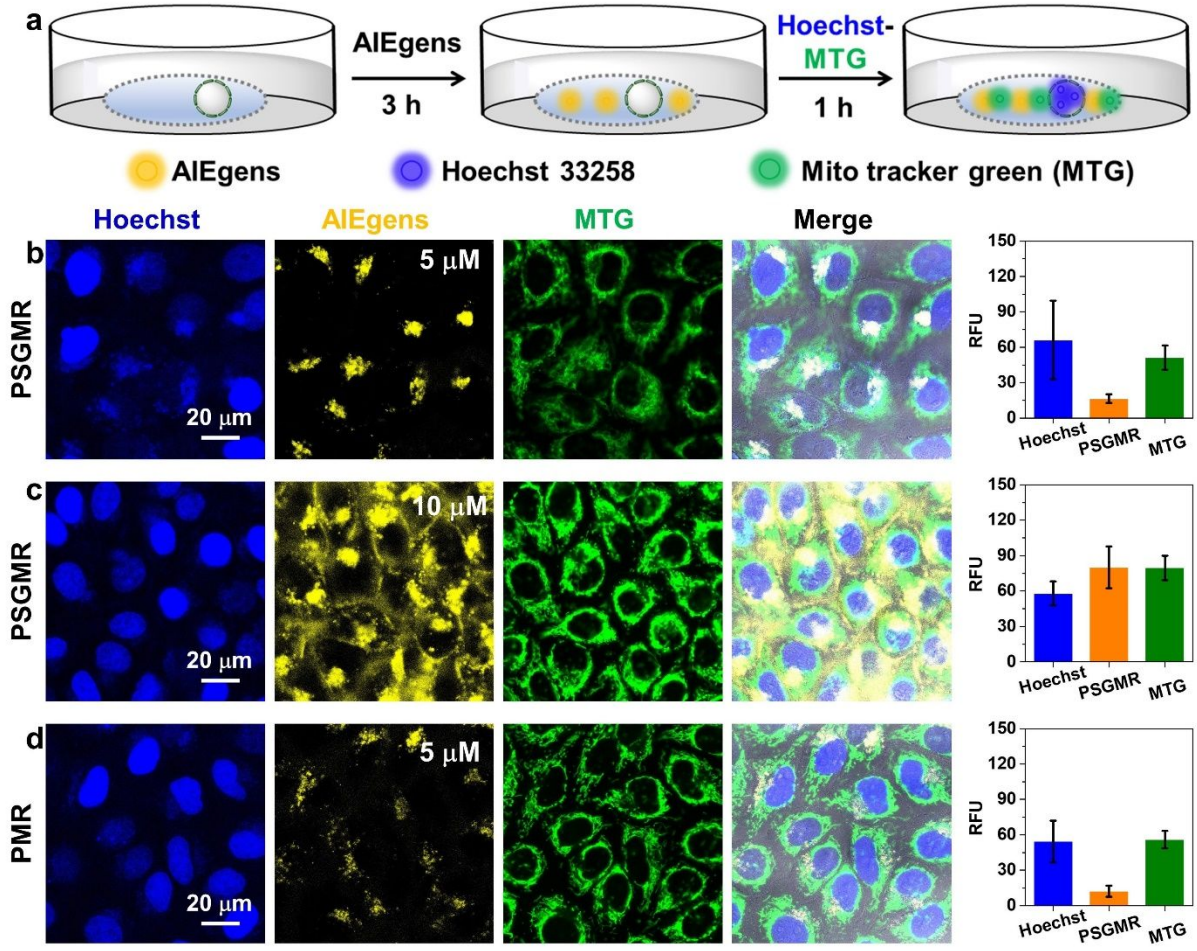

Figure S30. CLSM images and average fluorescence intensities of Hela cells incubated with PyTPE, PSGMR, and PMR for 3h, then added Hoechst 33258 and MTG for 1h.

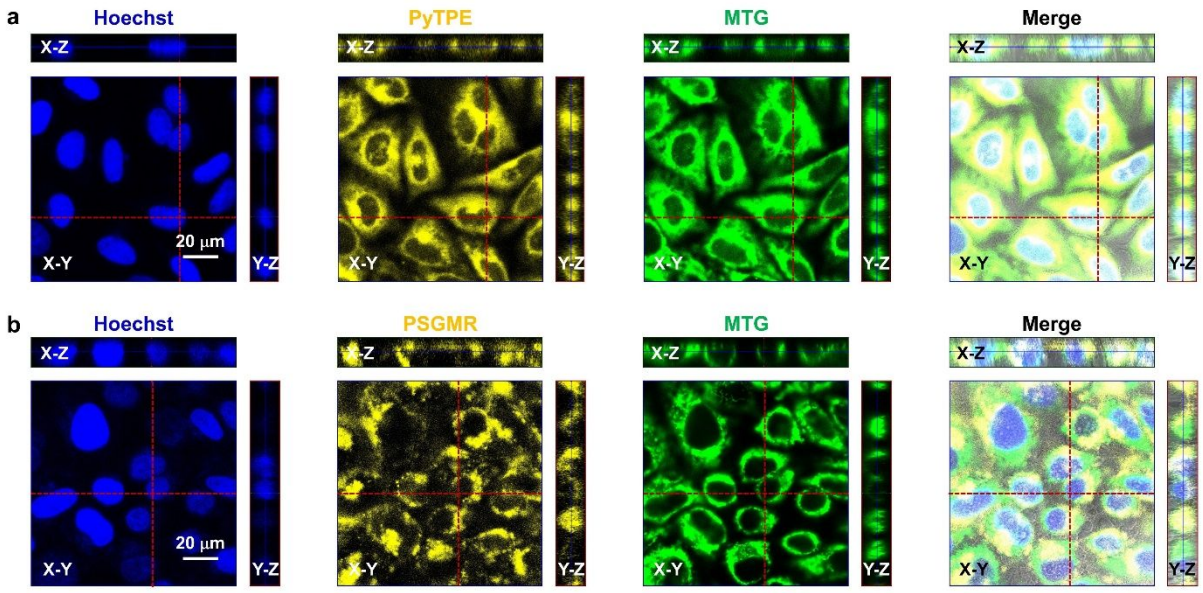

Figure S31. Z-stack images of Hela cells incubated with (a) 5 μM PyTPE and (b) 10 μM PSGMR for 3h, then added Hoechst 33258 and MTG for 0.5h.

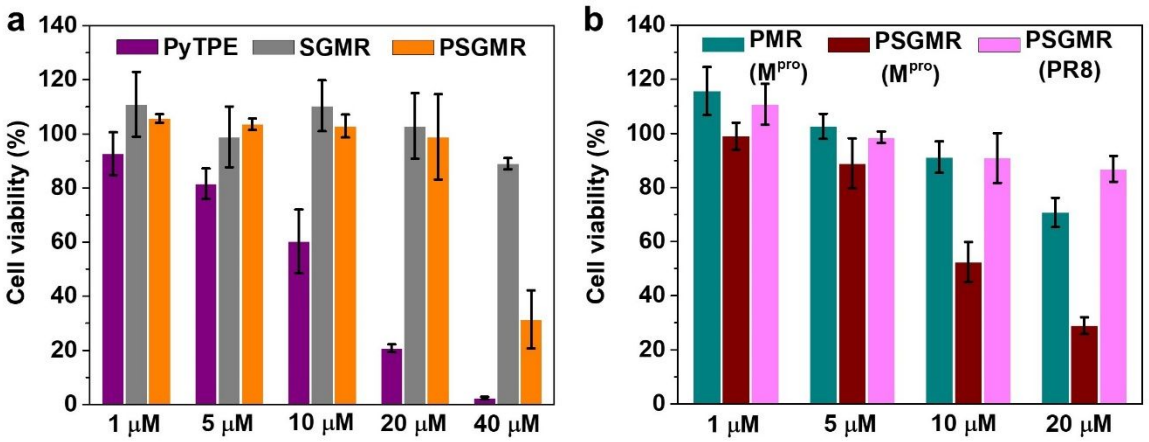

Figure S32. Metabolic activity of HEK 293T cells and plasmid transfected HEK 293T cells were studied with (a) (1 μM, 5 μM, 10 μM, 20 μM, and 40 μM) PyTPE, (1 μM, 5 μM, 10 μM, 20 μM, and 40 μM) SGMR, (1 μM, 5 μM, 10 μM, 20 μM, and 40 μM) PSGMR; (b) (1 μM, 5 μM, 10 μM, and 20 μM) PMR (M^{pro} plasmid), (1 μM, 5 μM, 10 μM, and 20 μM) PSGMR (M^{pro} plasmid), and (1 μM, 5 μM, 10 μM, and 20 μM) PSGMR (PR8 plasmid) for 48 h incubation using a fluorescence resazurin assay. The results show that the higher concentration of 10 μM of PyTPE and PSGMR (M^{pro} plasmid) are obviously cytotoxic.

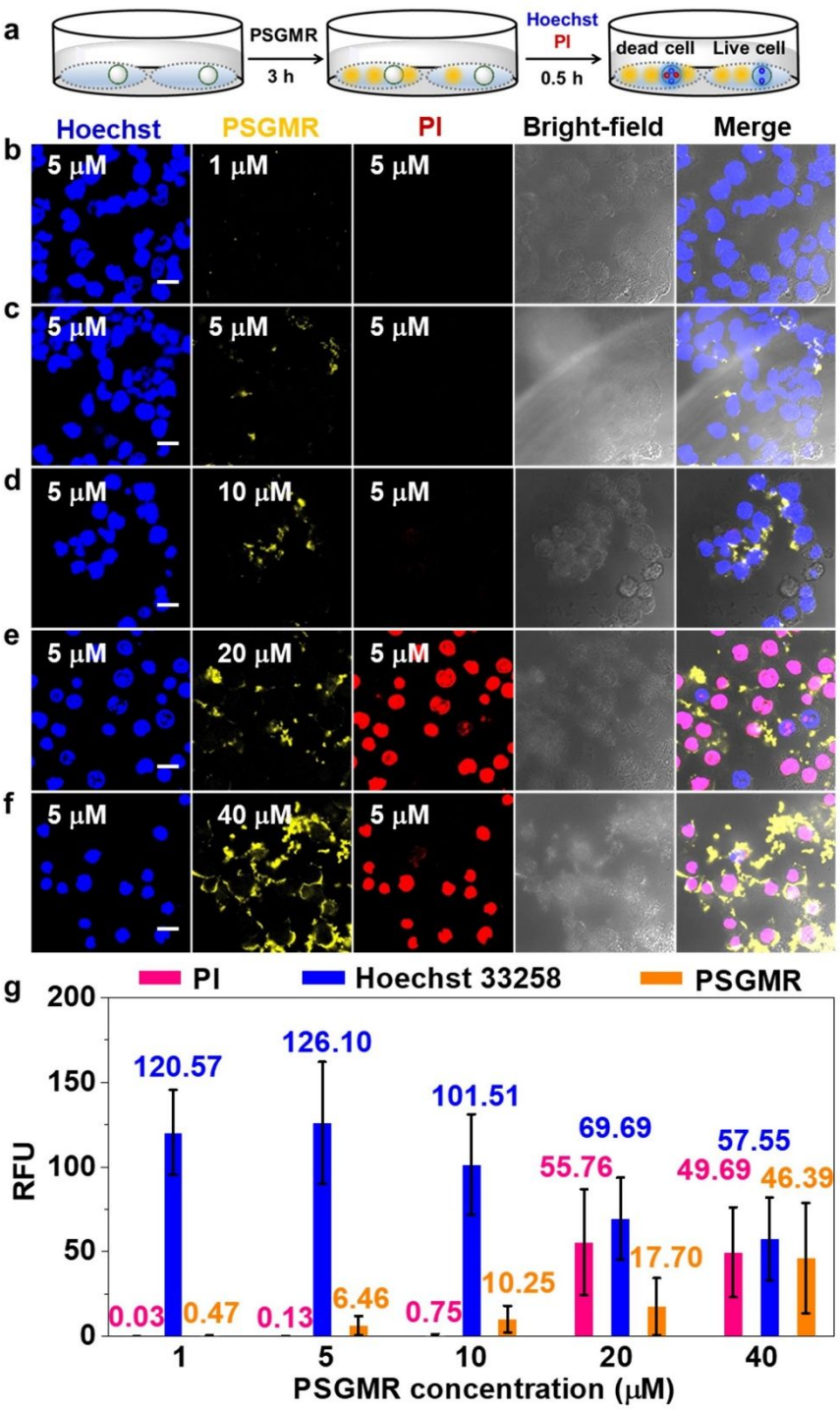

Figure S33. Confocal laser scanning microscopy (CLSM) images of HEK 293T cells incubated with Hoechst 33258, PSGMR, and PI. (a) The experimental scheme. Cell images of HEK 293T cells incubated with (b-f) 1 μM, 5 μM, 10 μM, 20 μM, and 40 μM PSGMR, 5 μM Hoechst 33258, and 5 μM PI for 3 h, respectively. (g) The average fluorescence intensities of HEK 293T cells incubation with Hoechst 33258, PSGMR, and PI. Scale bar = 20 μm.

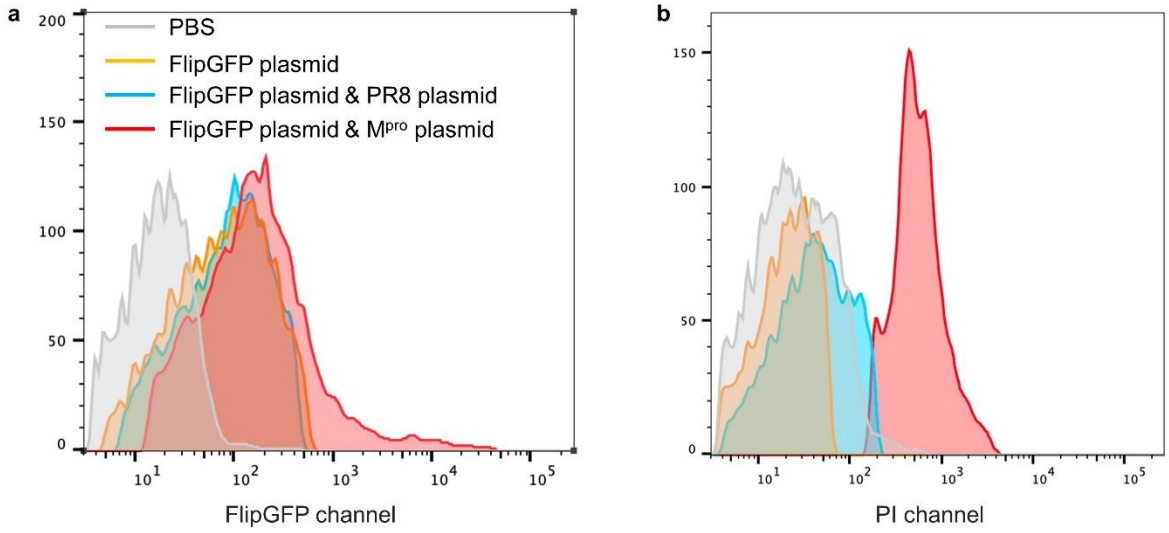

Figure S34. Flow cytometric analysis of FlipGFP plasmid, PR8 plasmid, and Mpro plasmid-transfected HEK 293T cells treated with 5 μM PSGMR for 1h, and PI for 0.5h. (a) FlipGFP channel, (c) PI channel. The gray, yellow, blue, and red parts represent the cells treated with PBS; FlipGFP plasmid; FlipGFP plasmid & PR8 plasmid; and FlipGFP plasmid & M^{pro} plasmid.

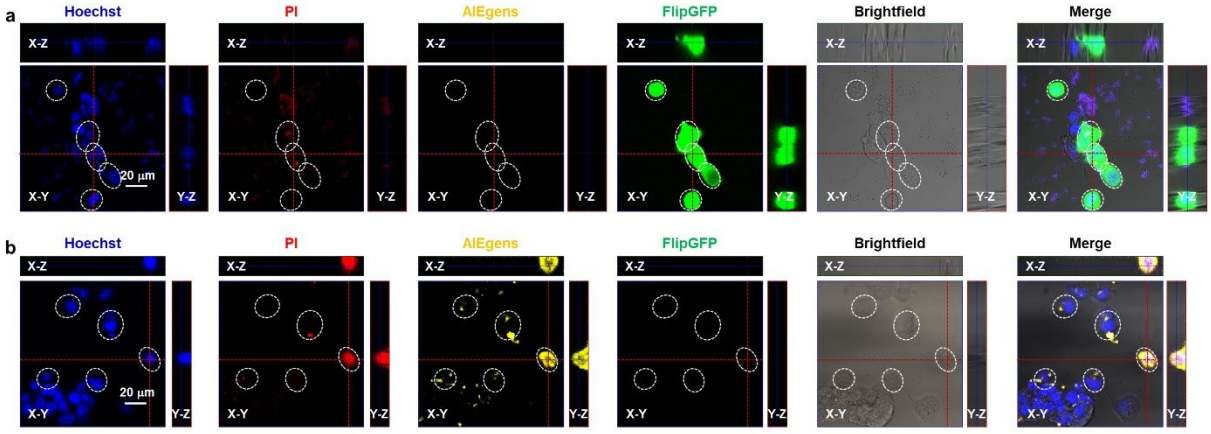

Figure S35. Z-stack images of M^{pro} plasmid-transfected HEK 293T cells incubated with (a) FlipGFP plasmid and (b) 5 μM PSGMR for 1h, then added Hoechst 33258 and PI for 0.5h.

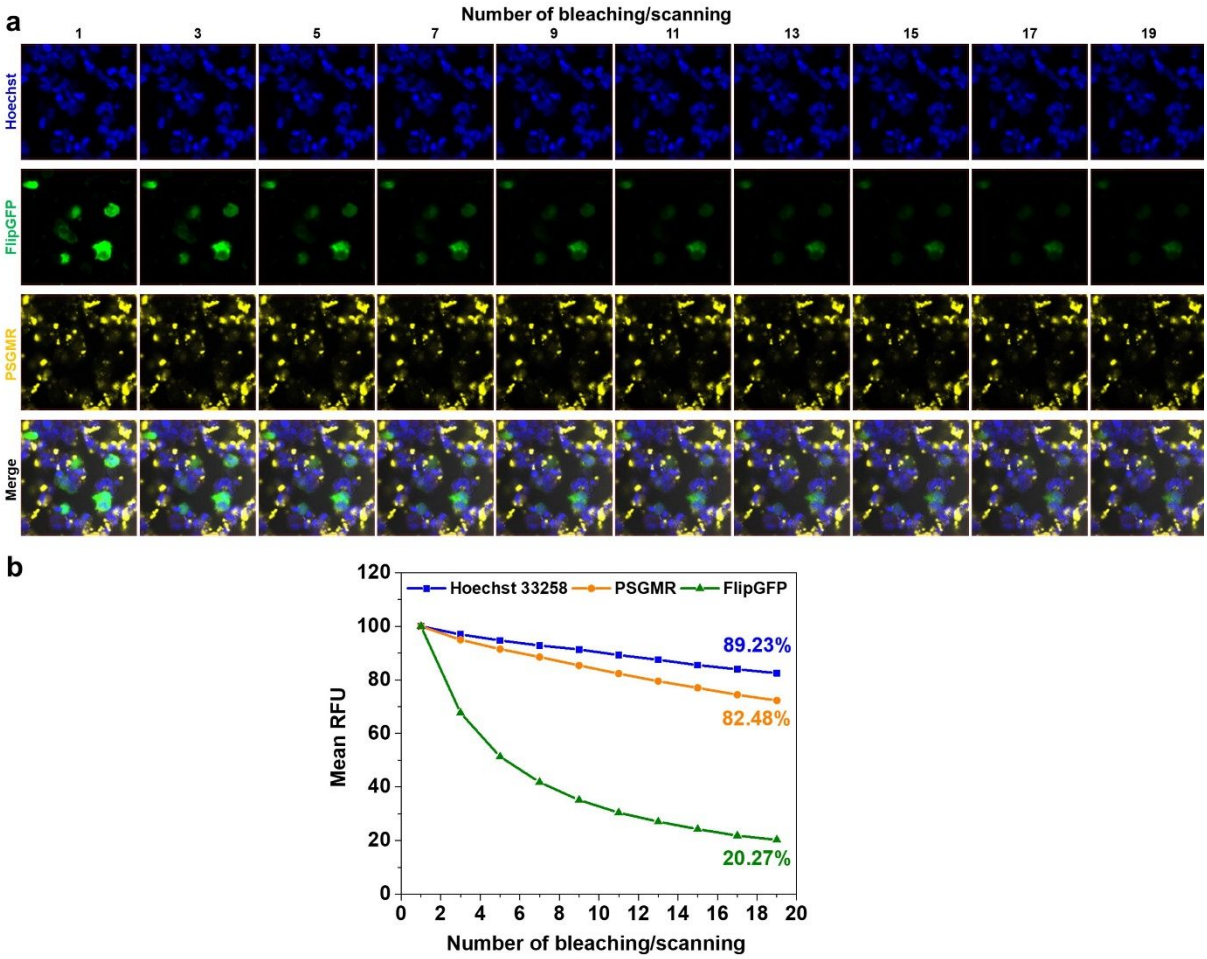

Figure S36. Photostability studies of M^{pro} plasmid- and FlipGFP plasmid-transfected HEK 293T cells incubated with 5 μM PSGMR and 5 μM Hoechst 33258 under an increasing number of bleaching events. (a) The corresponding CLSM images of HEK 293T cells and (b) the average fluorescence intensity changes of Hoechst 33258, PSGMR, and FlipGFP. bleaching wavelength: 405 nm and 488 nm; bleaching intensity: 100%.

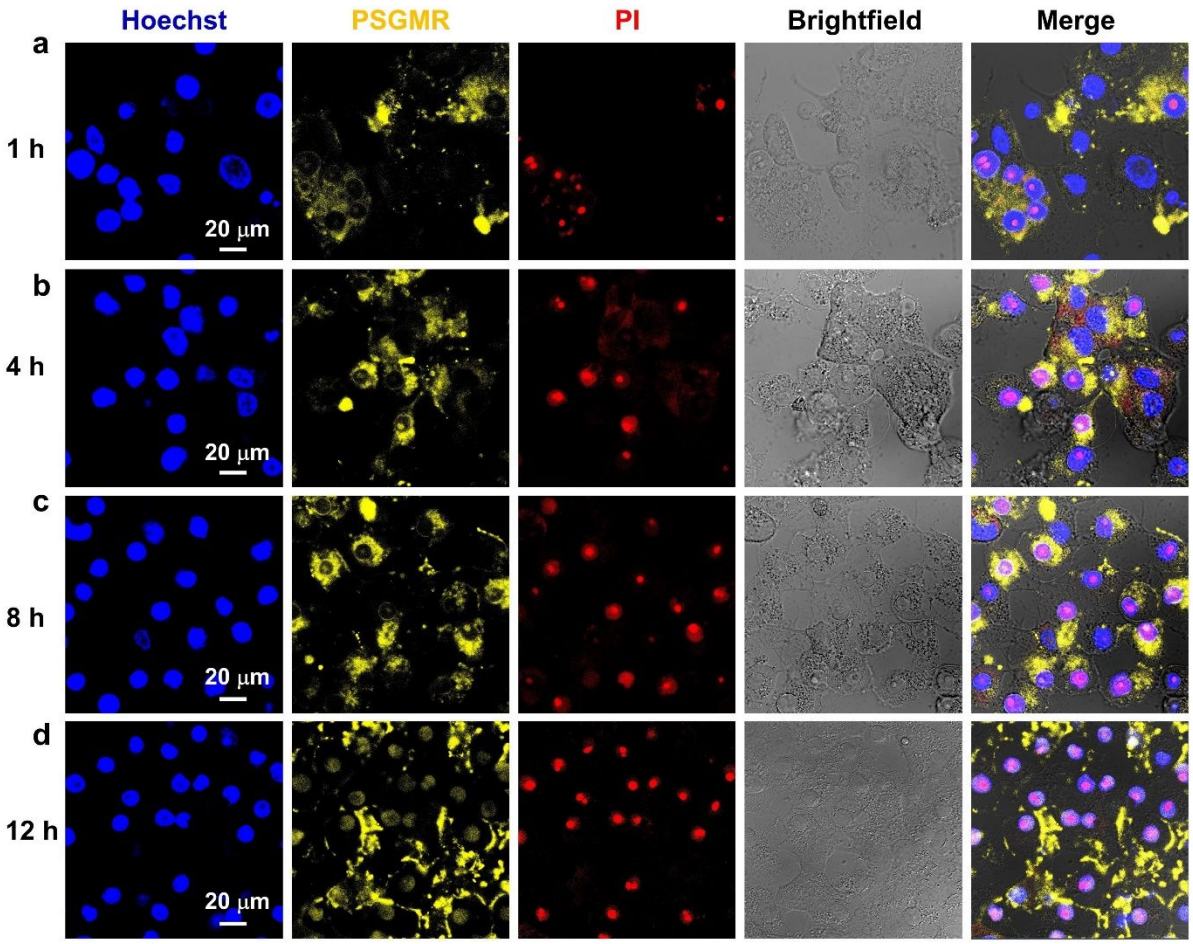

Figure S37. CLSM images of the M^{pro} plasmid transfected HEK 293T cells with 5 μM PSGMR, 5 μM Hoechst 33258, and 1 μM MTG for different time. Scale bar = 20 μm.

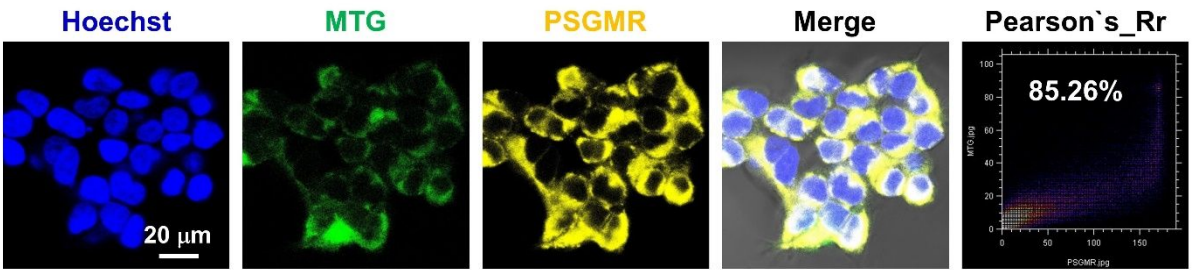

Figure S38. CLSM images and Pearson correlation coefficient of co-localization of the M^{pro} plasmid transfected HEK 293T cells with 5 μM Hoechst 33258, 1 μM MTG and 10 μM PSGMR. Scale bar = 20 μm.

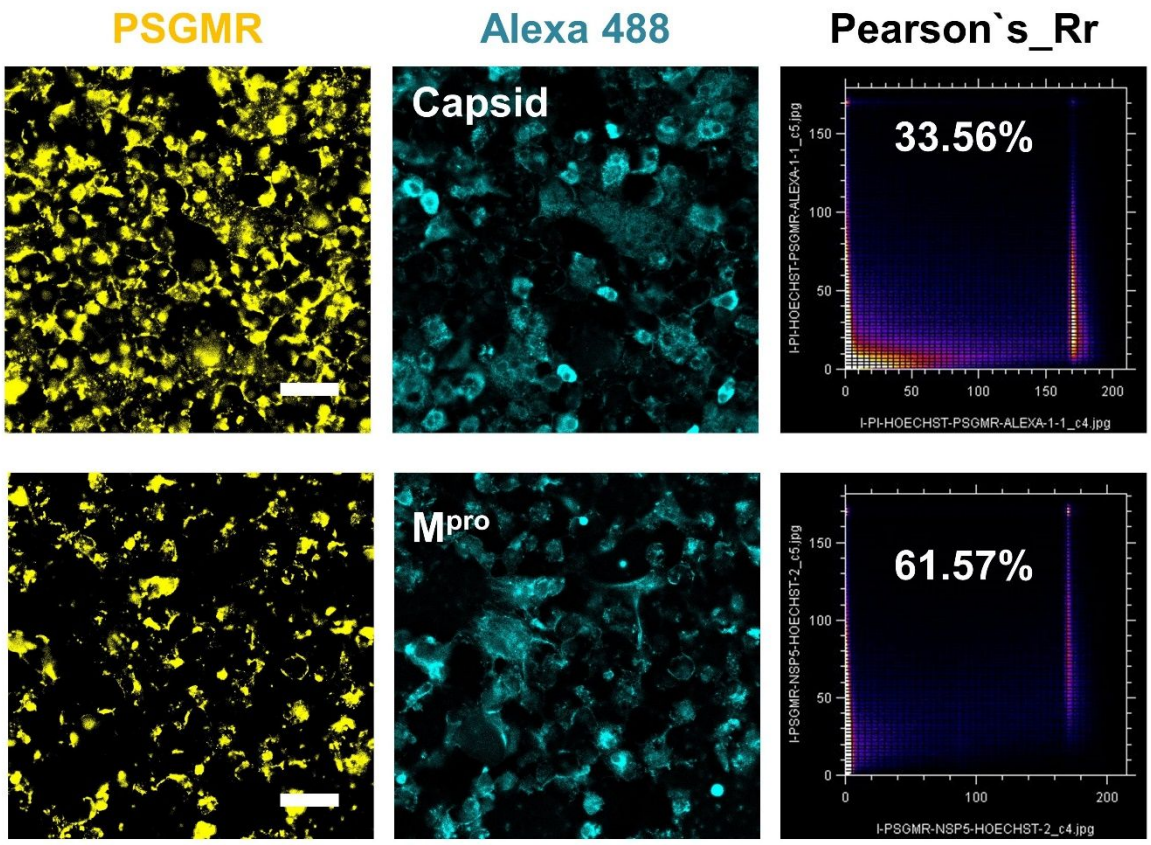

Figure S39. CLSM images and Pearson correlation coefficient of co-localization of the SARS-CoV-2-infected TMPRSS2-Vero cells with Alexa 488 (Capsid and M^{pro}) and 5 μM PSGMR. Scale bar = 50 μm.

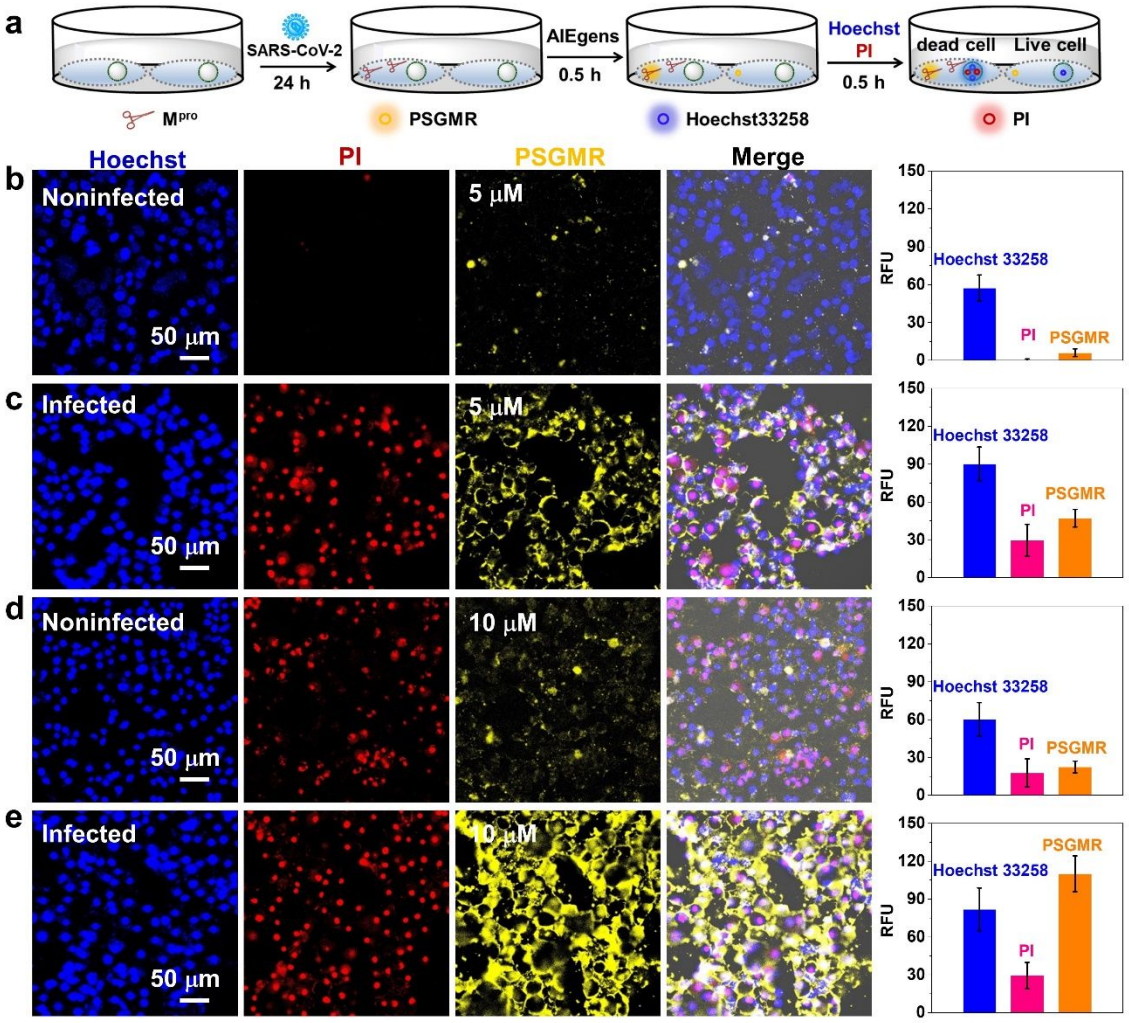

Figure S40. CLSM images and average fluorescence intensities of SARS-CoV-2 infected TMPRSS2-Vero cells incubation with Hoechst 33258, PI, and PSGMR. (a) The experimental scheme. Cell images and average fluorescence intensities of (b, d) noninfected TMPRSS2-Vero cells incubation with 5 μM and 10 μM PSGMR, and (c, e) SARS-CoV-2 infected TMPRSS2-Vero cells incubation with 5 μM and 10 μM PSGMR. Scale bar = 50 μm.

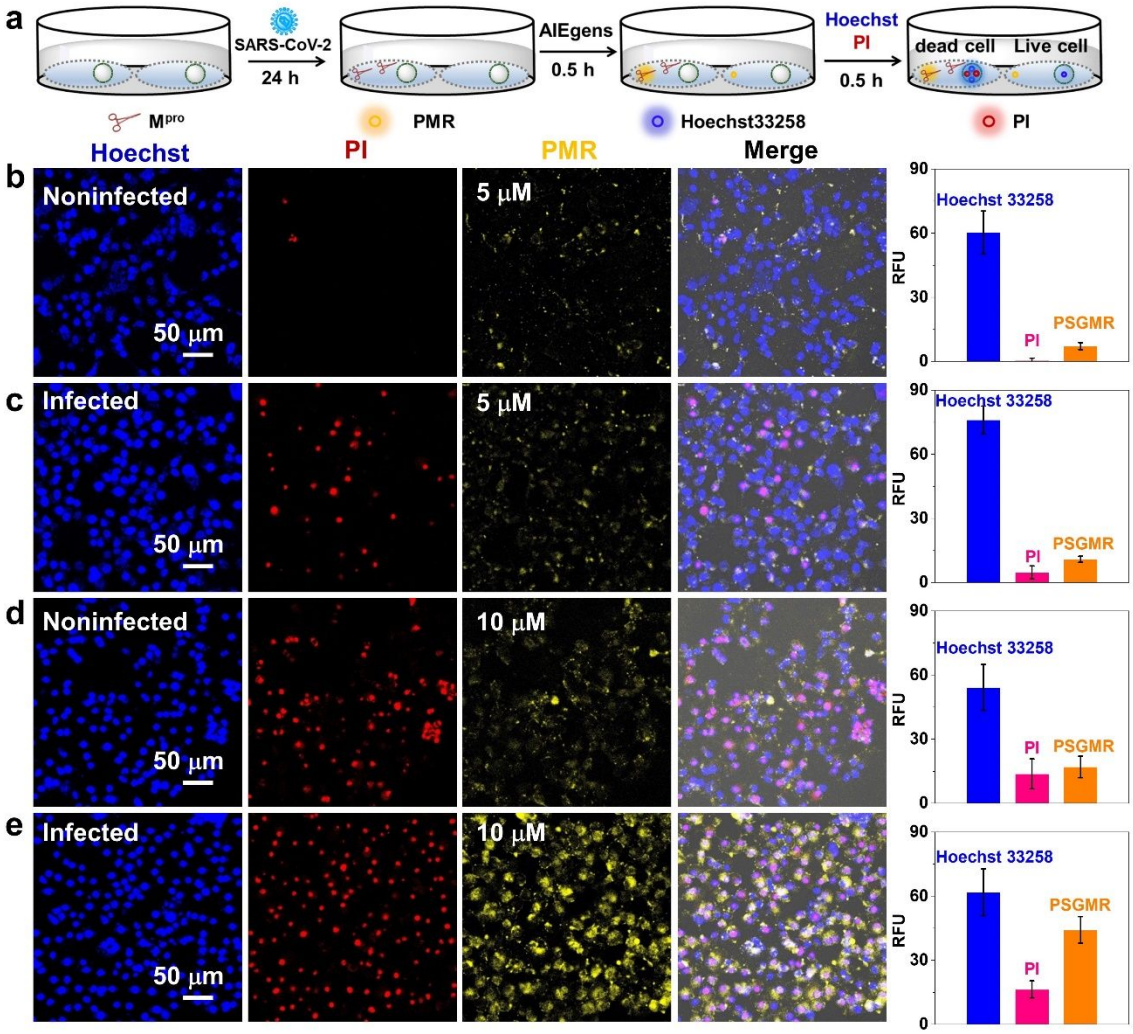

Figure S41. CLSM images and average fluorescence intensities of SARS-CoV-2 infected TMPRSS2-Vero cells incubation with Hoechst 33258, PI, and PMR. (a) The experimental scheme. Cell images and average fluorescence intensities of (b, d) noninfected TMPRSS2-Vero cells incubation with 5 μM and 10 μM PMR, and (c, e) SARS-CoV-2 infected TMPRSS2-Vero cells incubation with 5 μM and 10 μM PMR. Scale bar = 50 μm.

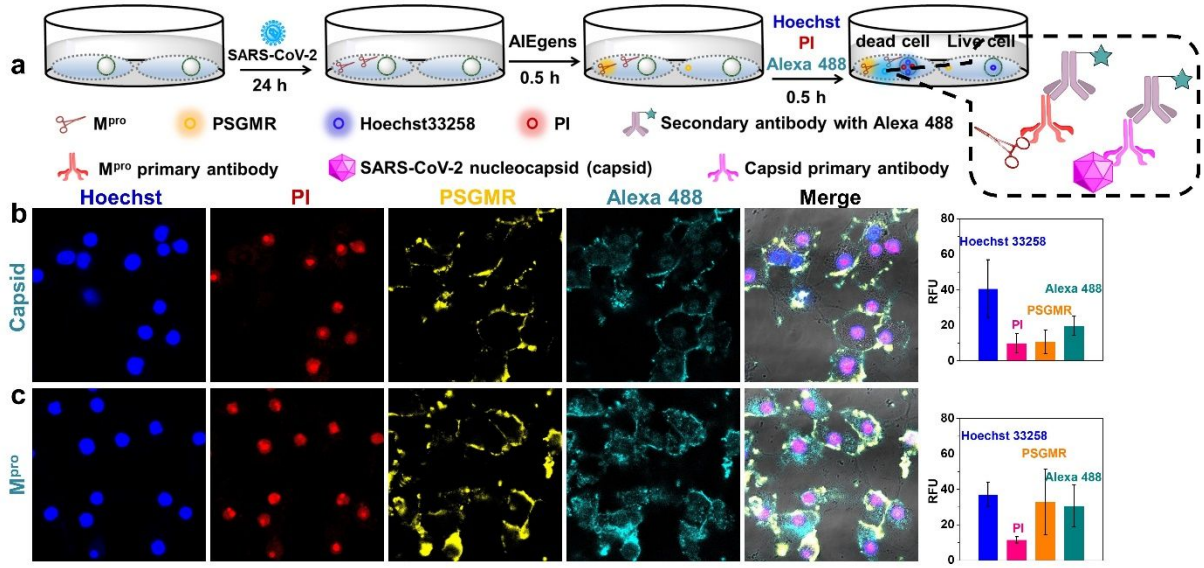

Figure S42. CLSM images and average fluorescence intensities of SARS-CoV-2 infected TMPRSS2-Vero cells incubation with Hoechst 33258, PI, PSGMR, anti-SARS-CoV-2 nucleocapsid (Capsid) primary antibody, anti-SARS-CoV-2 M^{pro} primary antibody, and AlexaFluor 488-labeled secondary antibody (Alexa 488). (a) The experimental scheme. Cell images and average fluorescence intensities of SARS-CoV-2 infected TMPRSS2-Vero cells incubated with 5 μM PSGMR, (b) anti-SARS-CoV-2 Capsid primary antibody/Alexa 488, and (c) anti-SARS-CoV-2 M^{pro} primary antibody/Alexa 488. Scale bar = 20 μm.

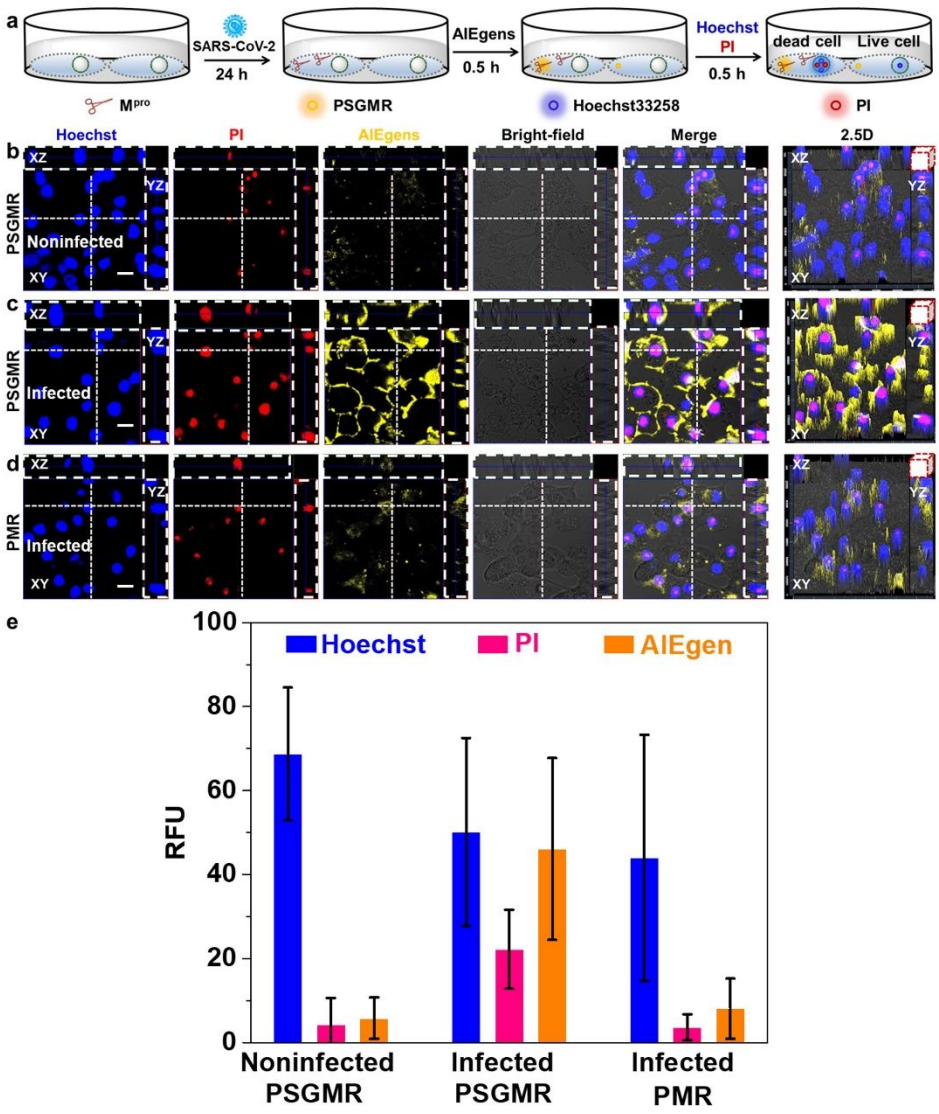

Figure S43. SARS-CoV-2 infected TMPRSS2-Vero cells incubation with Hoechst 33258, PI, PSGMR, and PMR. (a) The experimental scheme. (b) Noninfected cells incubated with PSGMR. (c) SARS-CoV-2 infected cells incubation with PSGMR. (d) SARS-CoV-2 infected cells incubation with PMR. (e) The average fluorescence intensities of TMPRSS2-Vero cells incubated with Hoechst 33258, PI, PSGMR, and PMR. Scale bar = 20 μm.

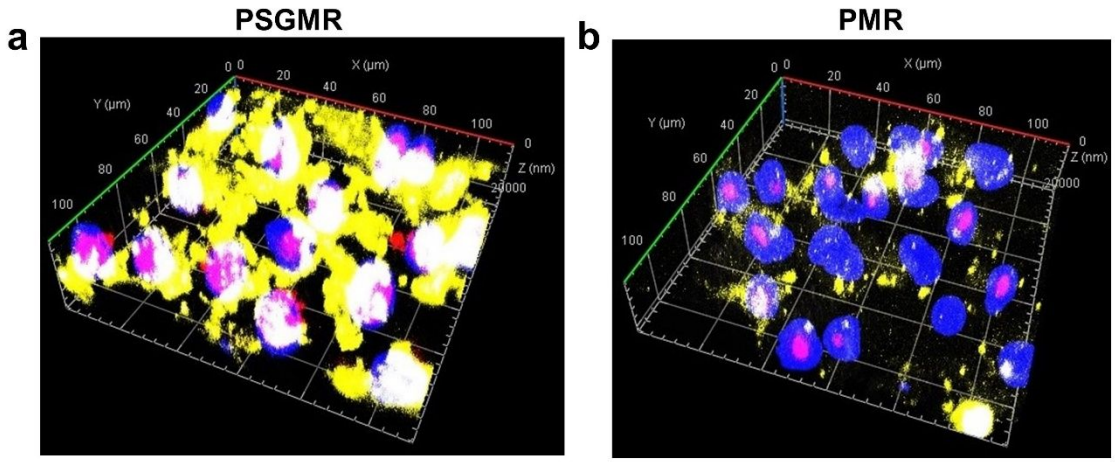

Figure S44. Corresponding the three-dimensional map of SARS-CoV-2-infected TMPRSS2-Vero cells incubated with 10 μM of (a) PSGMR and (b) PMR for 1 h.

References:

1. Mellott, D.M. *et al.* A Clinical-Stage Cysteine Protease Inhibitor blocks SARS-CoV-2 Infection of Human and Monkey Cells. *ACS Chem Biol* **16**, 642-650 (2021).
2. Froggatt, H.M., Heaton, B.E. & Heaton, N.S. Development of a Fluorescence-Based, High-Throughput SARS-CoV-2 3CLpro Reporter Assay. *Journal of Virology* **94**, e01265-01220 (2020).
3. Penalver, L. *et al.* A Ligand Selection Strategy Identifies Chemical Probes Targeting the Proteases of SARS-CoV-2. *Angew Chem Int Ed Engl* **60**, 6799-6806 (2021).
4. Cheng, Y. *et al.* Protease-Responsive Prodrug with Aggregation-Induced Emission Probe for Controlled Drug Delivery and Drug Release Tracking in Living Cells. *Anal Chem* **88**, 8913-8919 (2016).
5. Cheng, Y. *et al.* A Multifunctional Peptide-Conjugated AIEgen for Efficient and Sequential Targeted Gene Delivery into the Nucleus. *Angew Chem Int Ed Engl* **58**, 5049-5053 (2019).
6. Yi, X. *et al.* Self-Guiding Polymeric Prodrug Micelles with Two Aggregation-Induced Emission Photosensitizers for Enhanced Chemo-Photodynamic Therapy. *Acs Nano* **15**, 3026−3037 (2021).